Cell Genomics

Article

Transposable elements are associated with the variable response to influenza infection

Graphical abstract

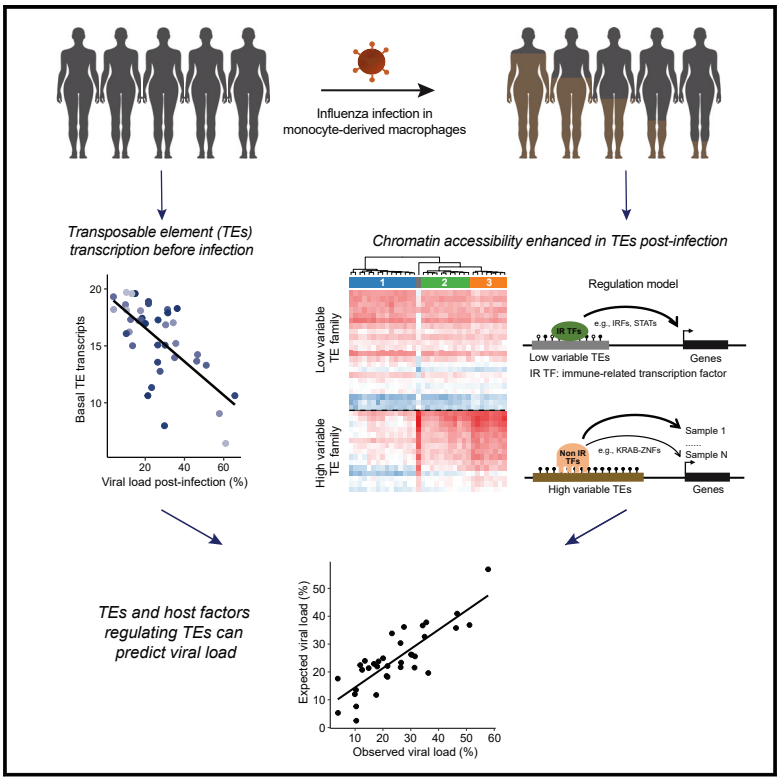

Highlights

- Several TE families had enhanced accessibility and variability following infection
- Basal TE transcripts level was inversely correlated with viral load post-infection
- Motif analysis revealed potential host regulatory factors, including KRAB-ZNFs
- TEs and associated host factors were predictive of viral load post-infection

Authors

Xun Chen, Alain Pacis, Katherine A. Aracena, ..., Tomi Pastinen, Luis B. Barreiro, Guillaume Bourque

Correspondence

guil.bourque@mcgill.ca

In brief

Using multi-omics data from monocyte-derived macrophages before and after influenza infection, Chen et al. characterize transcriptional and epigenetic changes in transposable elements (TEs). They identify epigenetically variable TE families with binding sites for novel host factors. Their findings suggest a role for TEs and KRAB-ZNFs in inter-individual variation in immunity.

Chen et al., 2023, Cell Genomics 3, 100292
May 10, 2023
https://doi.org/10.1016/j.xgen.2023.100292

CellPress

Cell Genomics

CellPress
OPEN ACCESS

Article

Transposable elements are associated with the variable response to influenza infection

Xun Chen,[1] Alain Pacis,[2] Katherine A. Aracena,[3] Saideep Gona,[3] Tony Kwan,[4] Cristian Groza,[5] Yen Lung Lin,[3] Renata Sindeaux,[6] Vania Yotova,[6] Albena Pramatarova,[4] Marie-Michelle Simon,[4] Tomi Pastinen,[7,8] Luis B. Barreiro,[3,9,10] and Guillaume Bourque[1,2,4,8,11,*]

[1]Institute for the Advanced Study of Human Biology (WPI-ASHBi), Kyoto University, Kyoto 606-8501, Japan
[2]Canadian Center for Computational Genomics, McGill University, Montréal, QC H3A 0G1, Canada
[3]Department of Human Genetics, University of Chicago, Chicago, IL 60637, USA
[4]Victor Phillip Dahdaleh Institute of Genomic Medicine at McGill University, Montréal, QC H3A 0G1, Canada
[5]Quantitative Life Science, McGill University, Montréal, QC H3A 1E3, Canada
[6]Centre de Recherche, CHU Sainte-Justine, Université de Montréal, Montréal, QC H3T 1C5, Canada
[7]Genomic Medicine Center, Children's Mercy Hospital and Research Institute, Kansas City, MO 64108, USA
[8]Department of Human Genetics, McGill University, Montreal, QC H3A 0C7, Canada
[9]Section of Genetic Medicine, Department of Medicine, University of Chicago, Chicago, IL 60637, USA
[10]Committee on Immunology, University of Chicago, Chicago, IL 60637, USA
[11]Lead contact
*Correspondence: guil.bourque@mcgill.ca
https://doi.org/10.1016/j.xgen.2023.100292

SUMMARY

Influenza A virus (IAV) infections are frequent every year and result in a range of disease severity. Here, we wanted to explore the potential contribution of transposable elements (TEs) to the variable human immune response. Transcriptome profiling in monocyte-derived macrophages from 39 individuals following IAV infection revealed significant inter-individual variation in viral load post-infection. Using transposase-accessible chromatin using sequencing (ATAC-seq), we identified a set of TE families with either enhanced or reduced accessibility upon infection. Of the enhanced families, 15 showed high variability between individuals and had distinct epigenetic profiles. Motif analysis showed an association with known immune regulators (e.g., BATFs, FOSs/JUNs, IRFs, STATs, NFkBs, NFYs, and RELs) in stably enriched families and with other factors in variable families, including KRAB-ZNFs. We showed that TEs and host factors regulating TEs were predictive of viral load post-infection. Our findings shed light on the role TEs and KRAB-ZNFs may play in inter-individual variation in immunity.

INTRODUCTION

Influenza A virus (IAV) infection causes seasonal epidemics worldwide and results in a wide range of disease severity between individuals. The underlying reasons for this variability remain largely elusive[1,2] but are determined by viral and host factors.[3] Indeed, viral determinants alone cannot account for the varied responses observed in individuals challenged by the same virus.[1,3,4] The human innate immune system, which involves the modulation of several cellular pathways, is a critical component of the response to infection.[5] Upon sensing of a virus such as IAV by recognition receptors, including RIG-I and TLR3, several signal transduction pathways are triggered that further modulate various transcription factors.[6–8] These regulators, including NF-kB/RELs, IRFs, and STATs, will engage the immune transcriptional network through the alteration of chromatin state, and in turn mediate the differential expression of hundreds of genes involved in the pro-inflammatory and antimicrobial programs to restrict virus replication and transmission.[9,10] Host factors involved in this cascade likely contribute to the variable response to IAV infection. Other factors also associated with influenza pathogenesis and that influence the response include pre-existing immunity, age, sex, obesity, and the microbiome.[3,11] Yet whether there exist other host factors that are important in determining the response to infection remains unknown.

Transposable elements (TEs), which occupy half of the human genome, play critical roles as *cis*-regulatory elements in various human biological processes.[12–14] Notably, a particular subclass of TEs, endogenous retroviruses (ERVs), are derived from ancient retroviruses and retain virus-like features that could stimulate the innate immunity, suggesting a potential association with infection and immunity.[15–17] Confirming this, an ERV family, MER41, contains regulatory sequences that are repurposed by the host to regulate host genes in the primate innate immune response.[18,19] TEs are also drastically upregulated in human immune cells upon extracellular stimuli, including viral infection.[20–24] Meanwhile, loss of SETDB1 or SUMO-modified TRIM28, which are associated with histone methylation and Kruppel-associated box domain (KRAB) zinc finger proteins

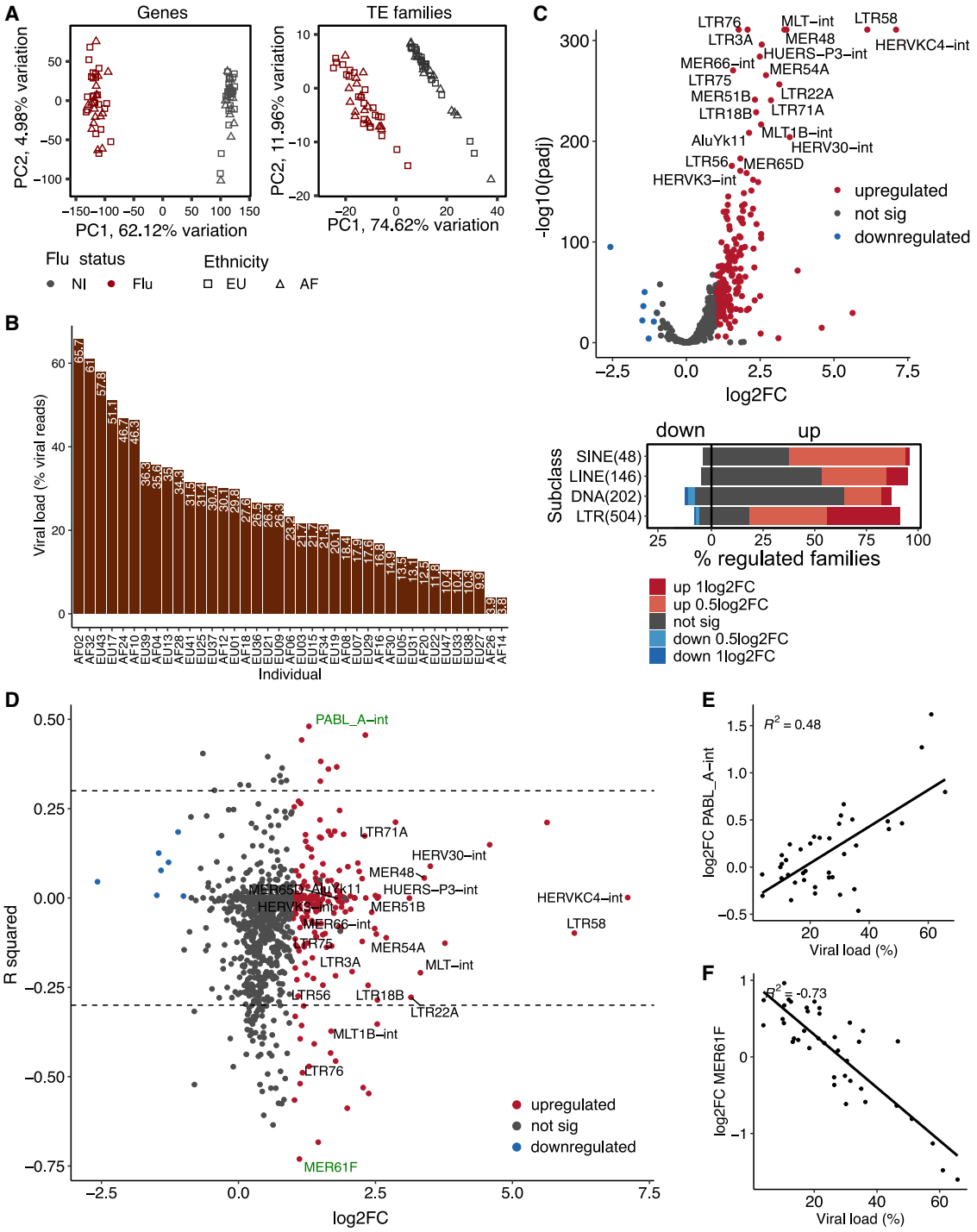

Figure 1. TEs are upregulated post-infection, but most expression changes are not correlated with viral load

(A) PCA plots of genes (left) and TE families (right) expression of individuals before and after infection. Individuals with African (AF) and European (EU) ancestry are indicated.

(B) Bar plots show viral load (percentage viral reads) across individuals post-infection.

(C) TE upregulation at the family level in human macrophages in response to IAV infection. Up-/downregulated families were detected as families with ≥ 1 $\log_2$ fold change ($\log_2$FC) in expression and adjusted p $\leq$ 0.001 upon infection (top). The highest 20 upregulated families on the basis of fold change are highlighted. The total number of examined families per TE subclass is indicated in parentheses. The vertical line separates the upregulated (left) and downregulated (right) families.

(legend continued on next page)

(ZNFs), leads to the de-repression of TEs.[23,25] Several studies have also suggested that upregulated TE transcripts may play a role in human innate immunity.[26,27] Moreover, given that many TE families have integrated after the divergence of primates from other mammals and are polymorphic in humans,[13] they could represent host factors contributing to the variable response to infection. Indeed, TE transcription is linked with aging[28–30] and microbiota,[31] which are associated with the response to infection.[3,11]

To test whether TEs and associated regulators are important host factors in the variable response to infection, we used data from a multi-omics study that profiled the transcriptome and epigenome before and after IAV infection in monocyte-derived macrophages derived from 39 individuals.[32] During the course of IAV infection, the amount of viral transcripts produced is variable and has been associated with disease severity.[1,33–35] Moreover, the number of viral reads observed in the macrophages post-infection can be used as a surrogate for viral load.[36] Indeed, in a similar experimental system this metric was shown to be stable and reproducible across individuals.[37] Notably, by studying the infected macrophages from these 39 individuals, we observed extensive variation in the levels of viral reads and discovered a set of TEs displaying high inter-individual variability in chromatin accessibility following infection. By looking for binding motifs in these variable regions we identified novel transcription factors likely contributing to the response to infection. Last, using TEs and these new host factors, we were able to build models that were predictive of the response to infection as measured by the number of viral transcripts.

RESULTS

Many TE families are upregulated following IAV infection, but few are correlated with viral load post-infection

To characterize individual differences in the response to IAV infection, we used RNA sequencing (RNA-seq) data obtained from monocyte-derived macrophages of 39 individuals before and after exposure to IAV for 24 h (Table S1; see STAR Methods and Aracena et al.[32]). As expected, we observed extensive gene expression changes upon infection (Figure 1A). Even though all samples engaged a strong transcriptional response to infection, we noticed extensive variation in the levels of viral reads (from 3.77% to 65.7%; Figure 1B), suggesting varying capacity for infection and/or to limit viral replication across individuals. Consistent with this hypothesis, viral load was inversely correlated with the expression fold change (FC) of several master regulators of the innate immune response, including transcription factors (TFs; e.g., *IRF3*, *STAT2*), adaptor molecules (e.g., *MYD88*, *TICAM1*) and interferon-inducible molecules (e.g., *IFNAR1*, *IFNAR2*) (Figure S1A). More globally, genes for which the transcriptional response to IAV infection was found to be correlated with viral load ($R^2 \geq 0.3$, $p \leq 0.05$; Figure S1B) were significantly enriched for pathways involved in the viral response. Like protein-coding genes, TE transcription levels were also significantly changed upon infection (Figure 1A). We inspected TE regulation at the level of families and identified 204 upregulated and seven downregulated families ($|\log_2 FC| \geq 1$, adjusted $p \leq 0.001$), respectively (Figure 1C; Table S2). In line with prior studies, we observed that ERVs (also known as LTRs) were the most commonly upregulated families (179 of 204 [85.5%]) and had the strongest FC (Figure 1C, bottom).

Next, we looked at the correlation between TE expression FCs and viral load post-infection. Among the 902 examined families, we only identified 17 and 77 families that were positively and negatively correlated with viral load ($R^2 \geq 0.3$, $p \leq 0.05$), respectively (Figure 1D; Table S3). For example, PABL_A-int was positively correlated with viral load (Figure 1E), while MER61F was negatively correlated with viral load (Figure 1F). Families from the LTR subclass, and ERV1 in particular, were slightly enriched for being positively correlated with viral load (Figure S1C). In contrast, families from the DNA subclass were prone to negatively correlate with viral load. Taken together, we observed significant upregulation of ERVs following IAV infection but the upregulation across individuals was correlated with viral load for only a small number of repeat families.

TEs contribute to dynamic chromatin regions in response to influenza infection

Beyond transcriptional changes, viral infection also induces significant epigenetic changes in immune cells.[10] We wanted to explore whether epigenetic profiles at TEs could help explain the inter-individual variability in the response to IAV infection. We used data profiling 35 of the 39 samples before and after infection using transposase-accessible chromatin using sequencing (ATAC-seq) and chromatin immunoprecipitation followed by sequencing (ChIP-seq) technologies characterizing various histone marks (Table S1; see STAR Methods).[32] Across these samples, we obtained an average of 137,478 peaks for ATAC-seq, 73,190 for H3K27ac, 230,292 for H3K4me1, 33,700H3K4me3, and 209,119 for H3K27me3 (Figure 2A; Table S4). The number of peaks across all marks was slightly higher in infected compared with non-infected (NI) samples. We observed that on average, 19.5%–47.6% of peaks were in TEs across marks (Figure 2B; Table S4). These proportions were found to be slightly but significantly increased post-infection for H3K4me3 and H3K27me3 ($p \leq 0.05$, Student's t test). To determine which regions were epigenetically variable between individuals, we measured the coefficients of variation (*cv*) in consensus peak regions[32] and identified similar proportions of variable regions in TE and non-TE regions for most marks (0.4%–6.4%, $cv \geq 0.5$; Figure 2C; see STAR Methods). Compared with non-TE regions, we observed higher variability of H3K4me3 (an average of 7.3% for TE and 3.6% for non-TE regions) and lower variability of H3K27me3 mark (0.3% for TE and 1.3% for

(D) Dot plots of correlation coefficients between TE FC and viral load post-infection. The x axis represents the $\log_2$FC of each family computed by DESeq2. The y axis represents the correlation coefficients (R^2, computed by linear regression model) between expression FCs and viral load among 39 individuals. The same 20 upregulated families (Figure 1C) are highlighted here. A positively and negatively correlated family (green) is shown as examples in (E) and (F), respectively.
(E) Example of positive correlation between PABL_A-int FCs and viral load.
(F) Example of negative correlation between MER61F FCs and viral load.

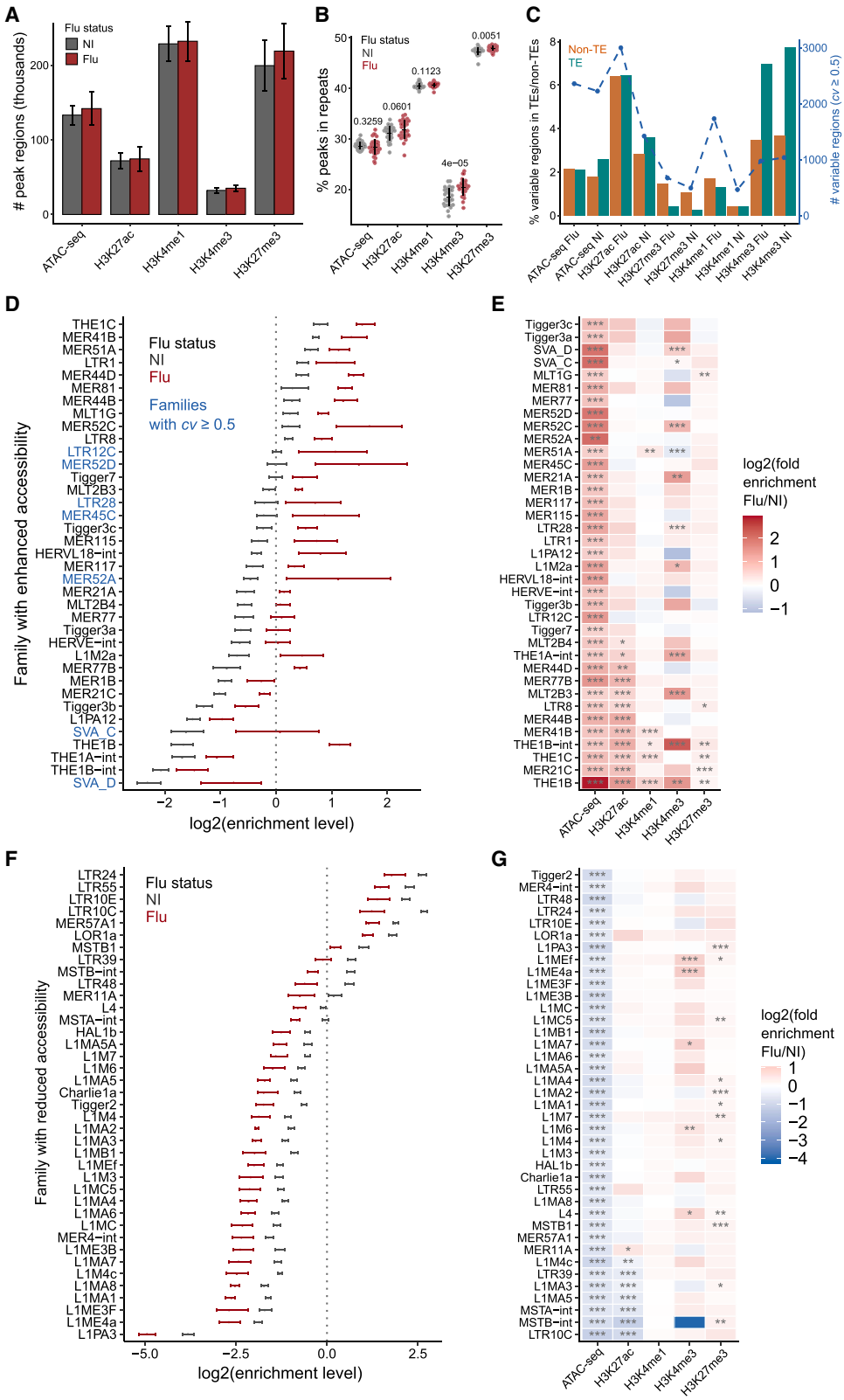

(legend on next page)

non-TE regions) in TEs, respectively. Given that H3K4me3 is typically associated with transcription, these results suggest variability of TE transcription before and after infection.

To explore the TE families with accessibility changes upon IAV infection, we compared the normalized number of accessible instances per family as measured by ATAC-seq in infected versus non-infected samples (Figure S2A). We identified 37 families with enhanced accessibility exhibiting 1.5-fold (adjusted $p \leq 0.05$) or greater abundance of peak-associated instances in infected relative to non-infected samples (Figure S2B; Table S5). For instance, we observed on average 584.2 peaks overlapping the THE1B repeat family in the flu samples, while only 79.5 were observed in the uninfected samples. The enrichment observed in these families can also be visualized relative to a random genomic background (Figure 2D) and include MER41B that was previously reported in K562, He-La, and CD14^{+} cell lines.[19] Notably, some families displayed a high degree of variation between samples post-infection (e.g., LTR12C, highlighted in blue). A similar analysis revealed that enhanced families were also frequently enriched for histone modifications, especially H3K27ac and H3K4me3 (Figure 2E). For instance, many H3K27ac peaks overlapped with THE1B and MER41B in infected samples (Figure S2C).

One of the advantages of comparing two conditions is that we could also look for TE families showing reduced accessibility upon infection. We identified 39 such "reduced families" (Figures 2F and S2D; Table S5). For instance, although on average 54.3 peaks overlapped L1M4c in non-infected samples, this number dropped to 26.0 in infected samples. Notably, 24 of the 39 (61.5%) reduced accessibility families were LINEs. This contrasts with the fact that only two out of 37 (1.7%) enhanced families were LINEs. Although some families with enhanced accessibility showed high variability between individuals, families with reduced accessibility displayed a uniform profile across most individuals (Figure 2F). Last, by inspecting the enrichments of other histone modifications, we identified seven families with reduced H3K27ac (Figure 2G; Table S5). Taken together, these results highlight many epigenetically changing regions of the human genome upon IAV infection are in TEs.

Several TE families display high inter-individual variability upon infection

Metaplots and heatmaps of chromatin accessibility further supported the high variability observed in some of the enhanced families post-infection. For instance, upon infection, THE1B (Figures 3A and S3A) showed less variation in chromatin accessibility across individuals than LTR12C (Figures 3B and S3A). To better understand why, we performed semi-supervised clustering analysis of the chromatin accessibility of the 37 enhanced families among the 35 infected samples (Figure 3C). This analysis revealed three groups of individuals post-infection. One outlier sample (EU37), was observed to consistently have the lowest fraction of reads in peaks (FRiP) scores among both infected and non-infected samples, suggesting a technical artifact rather than a biologically distinctive response to flu. Using this approach, a total of 15 enhanced families had the highest variability (Figure 3C, bottom), which we defined as "high variable families," especially between group 1 and group 3 individuals. In contrast, 22 enhanced families showed consistent enrichment patterns between three individual groups and were defined as "low variable families." A similar analysis in the non-infected samples did not reveal any groupings, suggesting an association specific to IAV infection (Figure S3B). Group 3 individuals tended to be slightly older and present higher viral loads compared with other groups, but the differences were not statistically significant (Figures S3C and S3D).

Next, we asked what fraction of repeat loci (instances) from the high variable families were contributing to the variability observed between individuals. Unsupervised clustering analysis of these loci revealed that many displayed high variability post-infection (Figure S3E). Among more commonly ($\geq$25% individuals of one group) and rarely (<25%) accessible instances from high variable families, we observed that they were often from group 3 individuals (Figure S4A; STAR Methods). To further identify features that were associated with variability in accessibility in TEs, we performed a comparative analysis between high and low variable families. We focused on flu-specific instances (ATAC-seq peak present in $\geq$1 infected but not in non-infected samples) and found that high variable families had a significantly higher proportion compared with low variable ($p = 2.4 \times 10^{-6}$, Student's t test) (Figures 3D and S4B). In contrast, we did not observe significant differences in the estimated evolutionary age (Figures 3E and S4C). Overall, compared with low variable families, we did find that high variable families had a significantly higher proportion of instances that overlap ATAC-seq peaks, that their repeat consensus

Figure 2. TEs contribute to dynamic chromatin regions in human macrophages in response to influenza infection

(A) Number of peak regions detected in infected and non-infected samples for ATAC-seq and histone marks.

(B) Proportion of ATAC-seq and histone marks peaks that overlap repeat regions. Two-tailed paired Student's t test was used to compare infected and non-infected samples for each mark.

(C) Number and proportion of variable peak regions overlap TE and non-TE regions. Variable regions were determined with the threshold of coefficient of variation (cv) $\geq$ 0.5 (see STAR Methods). Bars represent the proportions of peak regions that are variable, while the dotted line represents the corresponding peak counts. Infected (flu) and non-infected (NI) samples are shown separately.

(D and F) Distribution of $\log_2$ enrichment levels of families with enhanced (D) and reduced (F) accessibility in infected and non-infected samples. Candidate families were identified using the optimized methodology as we described in Figure S2A. The enrichment level refers to the fold enrichment per sample relative to the corresponding random distribution (see STAR Methods). Families with a high variability of enrichment levels between individuals (SD divided by the mean value, $cv \geq 0.5$) are highlighted in blue color (Table S5). The dotted line at "0" represents the random distribution. SDs were computed in non-infected and infected samples separately.

(E and G) Heatmap of $\log_2$ fold enrichments (flu/NI) of families with enhanced (E) and reduced (G) accessibility for ATAC-seq and each histone mark (i.e., H3K27ac, H3K4me1, H3K4me3, and H3K27me3). The fold enrichment was computed by dividing the average normalized number of peak-associated instances in infected by non-infected samples. Two-tailed paired Student's t test was used to compute the p values (*$p \leq 0.05$, **$p \leq 0.01$, and ***$p \leq 0.001$).

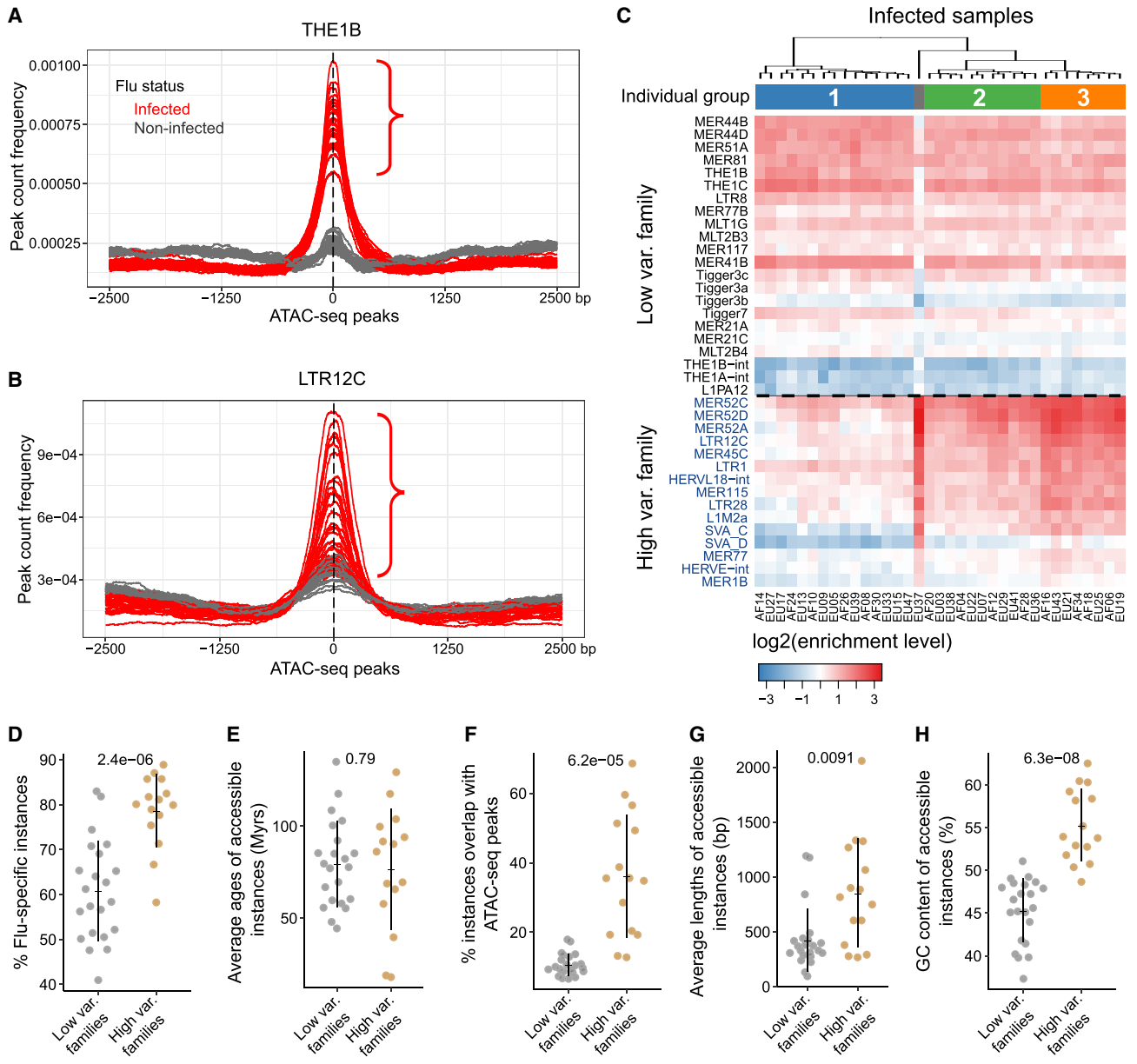

Figure 3. Uncovering a set of TE families that display high individual variability in chromatin accessibility post-infection

(A and B) Peak count frequency of ATAC-seq peaks overlapped with THE1B (A) and LTR12C (B). Red and gray lines represent the infected or non-infected samples. Compared with THE1B, LTR12C shows a higher SD between infected samples. Peaks overlapping each TE instance are centered at the median position of peak summits across samples. Upstream and downstream regions (2.5 kb) are shown.

(C) Heatmap of $\log_2$ enrichment levels of 37 families with enhanced accessibility in 35 infected samples. Semi-supervised clustering analysis was performed. Three individual groups are shown with an outlier sample. High variable families are highlighted in blue color and have higher enrichment levels in group 3 individuals than group 1 individuals. Enrichment level refers to the abundance of accessible instances in infected samples relative to the background.

(D–H) Comparative analysis of the proportion of flu-specific instances among all accessible instances (D), evolutionary ages (E), proportion of accessible instances among all instances (F), lengths (G), and GC contents (H) of accessible instances between high variable and low variable families. p values, computed using two-tailed Student's *t* test, are shown above the dot plots.

length was longer and that they had a higher GC content (Figures 3F–3H and S4D). Taken together, we identified 15 TE families with increased accessibility upon infection and high epigenetic variability between individuals and unique sequence features.

Enhanced and reduced TE families act as *cis*-regulatory elements in the response to influenza infection

Next, we asked if TE families with enhanced and reduced accessibility acted as *cis*-regulatory elements regulating nearby genes in response to IAV infection. We found that compared with

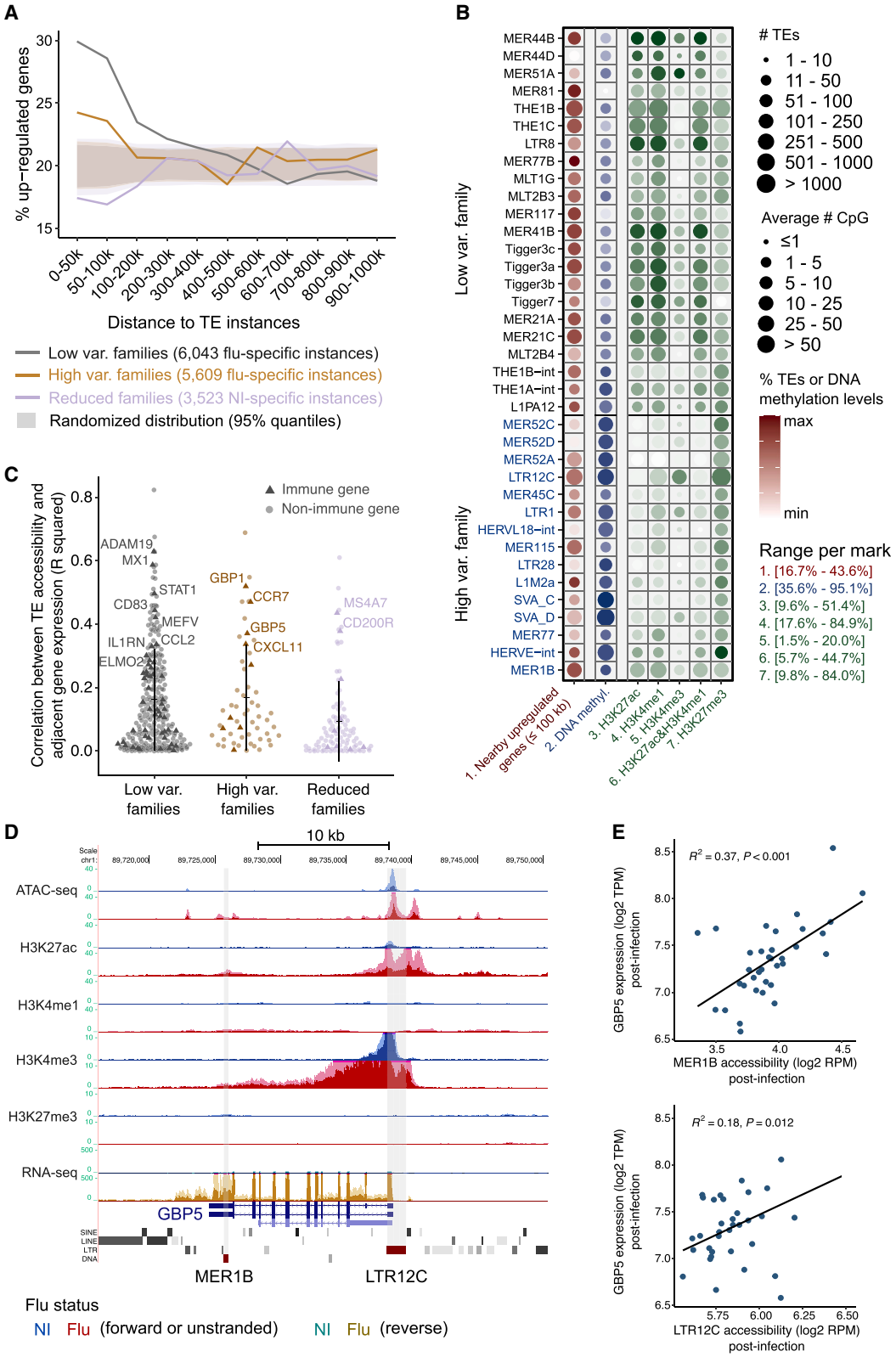

(legend on next page)

random genomic regions, upregulated genes were more likely to be located near instances from both low variable and high variable families that become accessible upon infection (flu-specific instances) (Figure 4A). Lower enrichments were observed for high variable compared with low variable families, indicating their weaker association to gene expression. In contrast, we observed a depletion of upregulated genes near non-infected-specific instances (accessible in $\geq$1 non-infected but not in infected samples) from TE families with reduced accessibility (Figure 4A). Notably, the opposite was observed for downregulated genes (Figure S5A). These effects were stronger for flu-/NI-specific instances compared with instances associated with shared peaks (Figure S5B). Splitting the enrichment at the TE family level, we observed consistent overrepresentation of accessible instances post-infection near upregulated genes within a 100 kb window for most enhanced families (Figure 4B, red color).

Next, we investigated the properties of chromatin post-infection more broadly by examining DNA methylation (Figure 4B, blue color) and sets of histone modifications (Figure 4B, green color). Instances from high variable families were highly DNA methylated (an average of 83.8%) and prone to overlap with H3K27me3 (47.3%), meanwhile they had a relatively small fraction of accessible instances overlapped with active marks (e.g., 15.1% for H3K27ac and 31.4% for H3K4me1). In contrast, low variable families were highly enriched for active histone marks (33.2% for H3K27ac and 60.7% for H3K4me1). Overall, low variable and high variable showed distinct chromatin patterns following infection suggesting different activation patterns and potential regulatory impact.

Finally, to further investigate which genes were potentially regulated by these TE-embedded sequences upon infection, we analyzed the list of nearby differentially expressed genes ($\leq$ 50 kb) and observed an enrichment in various immune-related pathways (Figure S5C). Next, we selected the repeat loci from the enhanced and reduced TE families with significant changes in accessibility and active histone modifications (H3K4me1 and/or H3K27ac). A total of 420 upregulated genes were found in proximity ($\leq$50 kb) to repeat loci from enhanced families and 168 downregulated genes from reduced families (Table S6). Of these, we found 17, 64, and 11 immune-related genes near instances from high variable, low variable, and reduced families, respectively. The correlation between the accessibility of many of these loci and their adjacent genes further supports coordinated regulation (Figure 4C). For example, *GBP5* gene is an interferon-induced gene and exhibits antiviral activity against viral infection.[38] An LTR12C instance and a MER1B instance with enhanced chromatin accessibility accompanied by an augmentation of H3K27ac and H3K4me1 upon infection can be found near this gene (Figure 4D). The accessibility of the two instances was positively correlated with *GBP5* expression level post-infection (Figure 4E). Furthermore, this specific LTR12C instance was previously validated to regulate *GBP5* expression in cell lines.[39] In a different LTR12C instance near the upregulated immune-related gene *IL10RA*, transcription was initiated at the open chromatin region within the repeat itself and was flu-specific (Figure S5D). We also confirmed the chromatin change at the LTR12C instance that was shown to be a promoter regulating *GBP2*[39] and a MER41 instance that was shown to be an enhancer regulating *AIM2* (Figures S5E and S5F).[19] Last, we identified several immune-related genes that were potentially regulated by adjacent instances from enhanced families, such as the TE gene pairs of MER52A-*GBP1/3*, LTR12C-*TRIM22*, THE1C-*IFI44*, THE1B-*PSMA5*, MLT2B3-*CLEC4E*, and tigger3a-*ADAM19* (Figures S5G and S5L). Thus, some of the instances from the enhanced and reduced TE families behave like *cis*-regulatory elements regulating nearby immune genes.

High variable families contribute transcription factor binding sites for potentially novel host factors in the response to infection

To look for regulatory proteins associated with enhanced and reduced families, we aggregated the reads in open chromatin regions across samples to fine-map the actual peak summit on each TE instance, which was termed a "centroid." After the removal of instances with inaccurate or inconsistent annotations (Figure S6A), we re-mapped the reads from each TE instance to its TE family consensus sequence. For example, we can visualize

Figure 4. TE families with accessibility changes may play critical regulatory roles in the response to influenza infection

(A) Fractions of upregulated genes near accessible TEs relative to the random distributions. Proportions of upregulated genes are shown within each of the genomic intervals relative to nearby accessible TEs. Flu-specific instances from high variable and low variable families and NI-specific instances from reduced families are considered. The total number of instances are indicated in the figure legend. Expected distributions were computed by randomizing each set of accessible instances 1,000 times (shaded area, 95% confidence intervals), suggesting a statistical significance of $p < 0.05$ for values outside the distributions. The proportions of upregulated genes are compared with corresponding expected distributions.

(B) Properties of high variable and low variable families overlapped with histone marks and DNA methylation. The number and proportion of accessible instances with nearest significantly upregulated genes within 100 kb ($\log_2$FC $\geq$ 0.5, adjusted p value $\leq$ 0.05) are shown in red color (first column). The number of CG sites and average DNA methylation levels are shown in blue color (second column). The number and proportion of accessible instances overlapped with each mark are shown in green color (third to seventh columns). The color ranges (proportion of accessible instances) are scaled by the minimum and maximum values for each mark.

(C) Correlation between the accessibility of TE-loci with significant changes of both accessibility (ATAC-seq) and active histone modifications (H3K4me1 and/or H3K27ac) and adjacent gene expression (within 50 kb) post-infection (see STAR Methods). Positively correlated upregulated genes are shown for enhanced families and downregulated genes are shown for reduced families. Strongly correlated immune genes ($R^2 \geq 0.3$, $p \leq 0.05$) are highlighted.

(D) Example genomic view of an accessible LTR12C instance and MER1B instance potentially upregulating adjacent *GBP5* gene expression post-infection. LTR12C and MER1B are highlighted as the shaded area with the increased accessibility, expression, H3K27ac, H3K4me1, and H3K4me3 activity. The dark shaded area denotes the distribution of the average reads per million (RPM) values and the light shaded area denotes the SD. Signals of various epigenetic marks are shown in blue color for non-infected samples and red color for infected samples. For RNA-seq, forward and reverse transcripts are shown in blue and green color separately for non-infected samples, while forward and reverse transcripts are shown in red and brown color separately for infected samples.

(E) Positive correlation between the accessibility of LTR12C and MER1B instances with *GBP5* expression level post-infection. R^2 and p values were computed by the linear regression model.

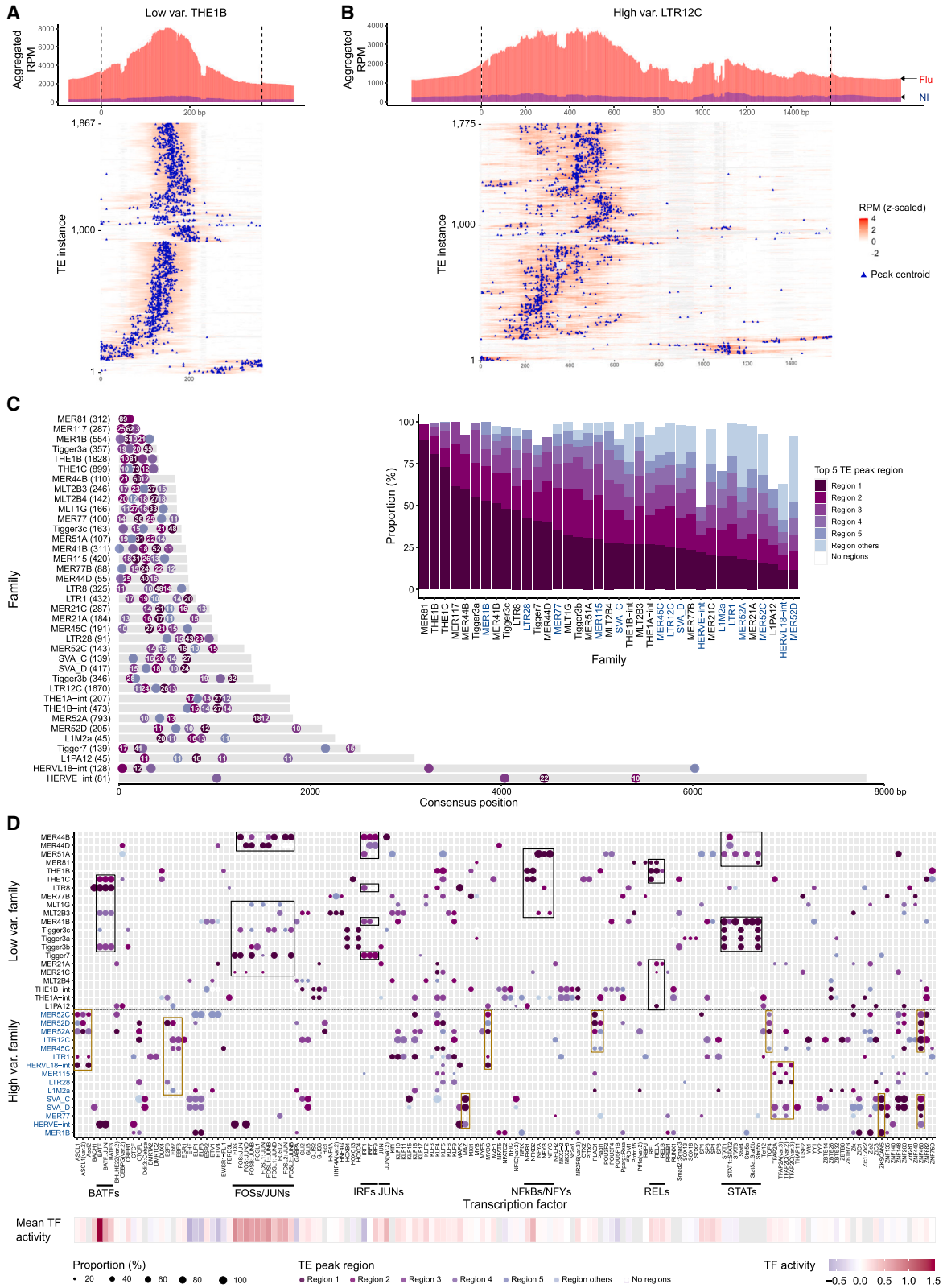

(legend on next page)

the peak centroids identified along the consensus sequences for THE1B, a low variable family (Figure 5A), and LTR12C, a high variable family (Figure 5B). We observed a higher complexity of open chromatin regions for LTR12C compared with THE1B. Centroids were mainly detected at about 180 bp for THE1B and were scattered between 150 and 600 bp for LTR12C. Next, we defined a ''TE peak region'' as a location on the consensus sequence containing peak centroids from five or more instances, starting with the region with the largest number of instances, named region 1, and so on. For most families, more than 80% of instances were accessible in one of the top 5 TE peak regions (Figure 5C, inset). The location of these TE peak regions can be shown on their consensus sequence and reveals that they are quite dispersed (Figure 5C). For example, 52% MER41B instances were accessible in region 1 located about 380 bp, while another 18% and 11% of them were accessible in region 2 (about 170 bp) and region 3 (about 570 bp) separately. Notably, compared with low variable families, high variable families had significantly more TE peak regions ($p = 0.022$, Student's t test) and lower proportions of accessible instances in the top TE peak region ($p = 0.0037$, Student's t test) (Figure S6B). This is consistent with the longer length of high variable families (Figure 3G).

To further investigate the molecular mechanism underlying the enhanced families, we examined the TF binding motifs that were enriched in each TE peak region (Figure 5D; Figure S6C). The enrichment of binding sites for STATs and IRFs in MER41B were previously reported.[19] Here we found that the STAT related motifs mainly came from MER41B instances that were accessible in region 1, while IRF-related motifs came from region 3. STATs were also observed in various Tigger3 and MER44 families, while IRF-related motifs were also enriched in various MER44 families, LTR8, and Tigger7. Other motifs of interest observed in consensus peak regions included FOSs/JUNs, BATFs, NFkBs/NFYs, and RELs. Notably, this instance-level motif analysis also revealed distinct sets of binding motifs between high variable and low variable families (Figure 5D). Specifically, low variable families were enriched for motifs of known immune regulators (e.g., BATFs, FOSs/JUNs, IRFs, STATs, NFkBs, NFYs, RELs), while high variable families were enriched for other motifs (e.g., ASCLs, CTCFs, EBFs, MAZ, MYOG, PLAGs, TFAP2s, various KRAB-ZNFs).

We speculated that the binding of TFs like KRAB-ZNFs may be associated with the individual epigenetic variability observed in high variable families post-infection. For example, by clustering accessible HERVE-int instances, we found that instances with peaks in regions 3 and 4, which were enriched for TFAP2 and ZNF460 motifs (Figures 5D and S6C), were prone to be accessible in group 3 rather than group 1 individuals (Figures S6D and S6E). Supporting the potential role of KRAB-ZNFs in high variable families, we observed that the binding sites for KAP1 and multiple ZNF TFs[40] were enriched in some high variable families (Figure S7A; Table S7); Moreover, the binding regions significantly overlapped the open chromatin regions in some high variable families post-infection (Figure S7B). Because of the limited number of KRAB-ZNF motifs in the JASPAR database, we used another source of KRAB-ZNF motifs[41] to identify motifs across the accessible instances from enhanced families. We observed enrichment of KRAB-ZNF motifs in high variable families but not in low variable ones (Figure S7C; Table S7). KRAB-ZNFs are commonly found to interact with the KAP1/TRIM28 machinery to repress TEs through DNA and histone repression,[42,43] thus the enrichment of KRAB-ZNF binding sites and motifs in high variable families is also consistent with the high DNA and histone repression observed in these families (Figure 4B).

Finally, we performed a similar analysis to examine the TE peak regions and corresponding motifs enriched in the 39 families with reduced accessibility (Figures S8A and S8B). We identified the enrichment of IRF1, MEF2A/B/C/D and SPI related motifs in these families. Notably, L1MA2, L1MA4, L1MA6, L1MA7, and L1MA8 were significantly enriched for MEF2 related motifs. MEF2 TFs are central developmental regulators,[44] which are also required in the immune response that functions as an *in vivo* immune-metabolic switch.[45] Last, by further inspecting TFs with their binding motifs that were enriched in enhanced and reduced TE families, we found that TFs bound to high variable families were mainly enriched in transcription-related pathways while TFs bound to low variable and reduced families were mainly enriched in immune-regulated pathways (Figure S8C). Taken together, we concluded that high variable families have a unique profile and are associated with potentially new host factors, including KRAB-ZNFs.

TE-associated host factors can be used to predict viral load post-infection

Finally, we asked whether TE and TE-associated host factors can be predictive of viral load post-infection. As we previously

Figure 5. Low variable and high variable families contribute binding sites for distinct sets of potential host factors in the response to infection

(A and B) Distribution of chromatin accessibility along the THE1B (A) and LTR12C (B) consensus sequence. Distribution plots (up) show aggregated (summed) reads per million (RPM) values across accessible instances. Infected and non-infected samples are shown separately. Upstream and downstream regions (±20% of the consensus sequence length) are shown. Heatmaps (bottom) show *z*-scaled RPM values per accessible instance. In the heatmap, scaled RPM values below zero are shown in white color and the deletions relative to the consensus sequence are shown in gray color. The centroid (blue triangle) refers to the peak summit per instance. The total number of instances are indicated as the y axis.

(C) Distribution of TE peak regions on each enhanced family. A TE peak region was previously defined as a location within a TE that has a peak centroid in ≥5 instances. Here, the locations and proportions (%) of the top-five TE peak regions are shown on each consensus sequence. The number in each dot refers to the proportion among accessible instances (≥10%) in each TE peak region. The y axis shows the family name, consensus name, and the number of accessible instances in TE peak regions. The inset bar plot shows the proportion of instances in each TE peak region. Region 1 represents the TE peak region with the highest proportion, region 2 refers to the second highest, and so on. High variable families are in blue color.

(D) TF binding motifs enriched in enhanced families. Same motifs enriched across TE peak regions are aggregated. TE peak regions with the most number of instances are shown as representatives. Black boxes highlight candidate motifs recognized by known immune regulators enriched in low variable families; brown boxes highlight top candidate motifs recognized by potential novel host factors enriched in high variable families. High variable families are highlighted in blue color. Mean TF activity was obtained from Aracena et al.[32] Missing values are in gray color.

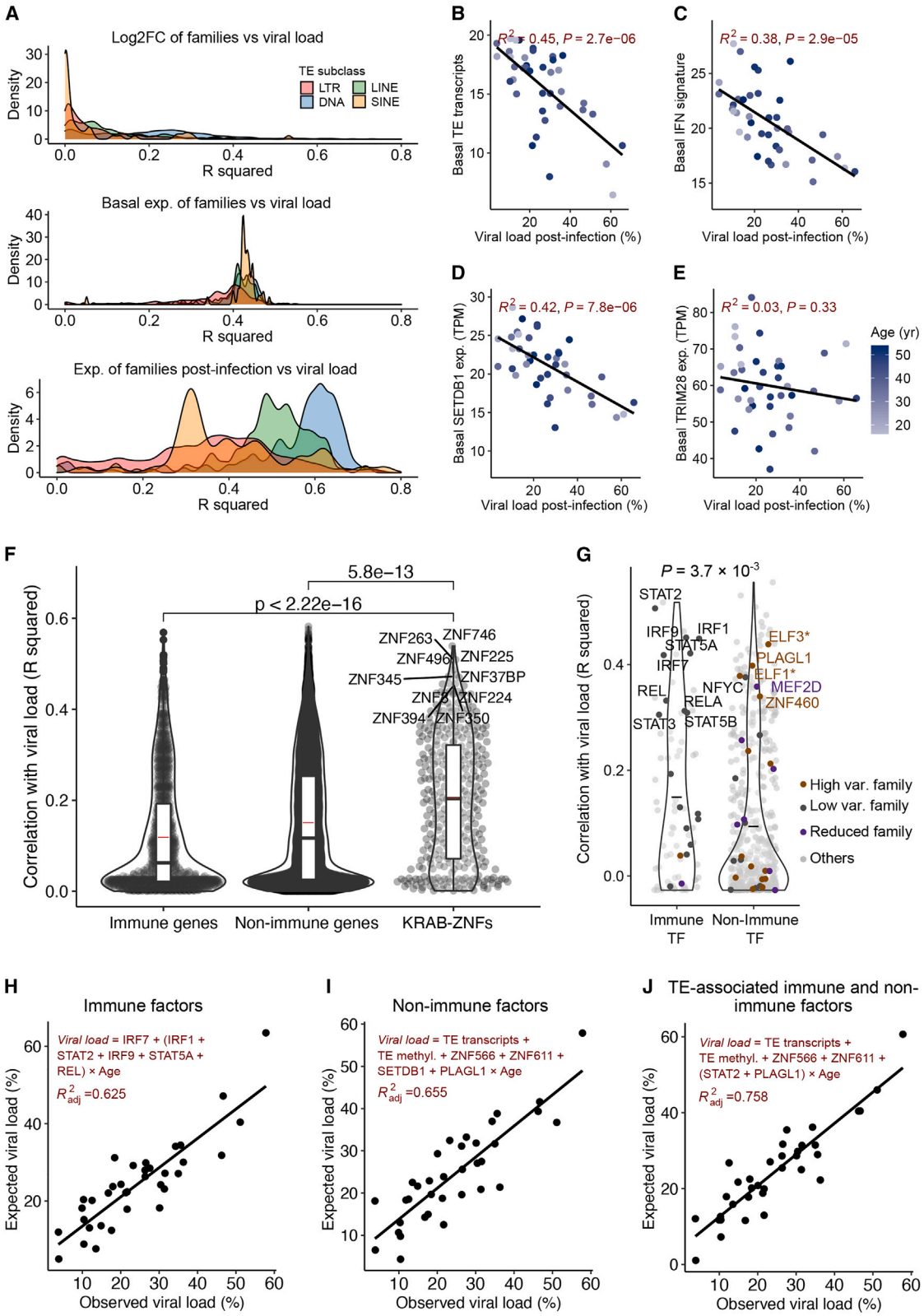

(legend on next page)

noted, the expression changes of most TE families were not correlated with viral load (Figure 1D), however, we further inspected the TE expression levels in non-infected and infected samples, respectively. Unlike expression changes, we observed that the basal and post-infection expression levels of many families were correlated with viral load (Figures 6A and S9A; Table S3). Basal expression of most TE families had comparable correlation coefficients, in contrast to post-infection expression levels. Combining reads across families, we found that there was a strong inverse correlation between the total amount of basal TE transcripts and viral load post-infection (R^2 = 0.45, p = 2.69 × 10^{-6}; Figure 6B). Inverse correlations were also observed for each of the four main TE subclasses (Figure S9B). As expected, the basal activation of the immune system (interferon signature) was also inversely correlated with viral load (Figure 6C; R^2 = 0.38; see STAR Methods).

To explore the role of other factors known to be associated with the regulation of TEs, we inspected both *TRIM28* and *SETDB1*. We first examined the FC and observed a strong correlation to viral load post-infection for *SETDB1* but not for *TRIM28* (Figure S9C). Similarly, an inverse correlation was observed between *SETDB1* basal expression and viral load (R^2 = 0.42, p = 7.83 × 10^{-6}) but not for *TRIM28* (R^2 = 0.026, p = 0.32) (Figures 6D-6E). We then examined the basal expression levels of all KRAB-ZNFs and observed a significantly higher correlation with viral load compared with immune and non-immune-related genes (Figure 6F; Table S7). Next, looking at the average DNA methylation in TEs pre-infection, we did not observe a correlation with viral load (Figure S7D). Age is another factor that is potentially associated with TEs, even though it was not observed to correlate with viral load in our data (Figure S9E). We noted that the variability of basal TE transcription increased as the age increased (Figure S9E). Actually, the inverse correlation observed between basal TE transcripts and viral load became even stronger (R^2 = 0.76, p = 4.6 × 10^{-7}) with the exclusion of individuals older than 40 years old (Figure S9F).

We continued our analysis of the host factors that are associated with epigenetic variability in high variable families. First, we examined the correlations between basal expression levels of all expressed TFs and viral load (Figure 6G). As expected, known immune-related TFs had higher correlation coefficients with viral load compared with non-immune TFs (p = 3.7 × 10^{-3}). Focusing on TFs associated with enhanced and reduced TE families, we found that many were strongly correlated with viral load (Figure 6G). We further found that the expressions of ten KRAB-ZNF genes were strongly correlated with the aggregated accessibility of high variable families post-infection (Table S7; $R^2 \geq 0.3$, $p \leq 0.05$). After integrating these results, we identified *PLAGL1* and three KRAB-ZNFs (i.e., *ZNF519*, *ZNF566*, and *ZNF611*) as top candidate host factors (Figure S9G; Table S7). Notably, *PLAGL1*, which is a family member of *PLAG1*, also encodes a C2H2 zinc finger protein that could be repressed by SUMOylation.[46]

Last, we wanted to test our ability to combine all this information into predictive models to estimate the variable responses to IAV infection. We started with IFN related features as variables including the IFN signature and age to achieve a model explaining 36% of the variation (Figure S9H). Next, we included the top six immune factors bound to low variable families that were correlated with viral load as variables and used a stepwise approach to select the final set of features in a generalized linear model (see STAR Methods). Age was also included as an interaction term variable because of its influence on multiple variables. Using this approach, we were able to build a better model (adjusted R^2 = 0.625) (Figure 6H). Afterward, we looked at all the TE-related host factors described above in a correlation matrix chart with viral load (Figure S9I). Notably, when we included six non-immune factors associated with TEs and age in our model,

Figure 6. TEs and TE-associated host factors are predictive of viral load post-infection

(A) Distribution of correlation coefficients (R^2) between the TE expression level (TPM) in non-infected and infected samples and TE expression fold changes with viral load post-infection. Log_2FCs and TPM values were calculated as we previously described. Four TE subclasses are shown separately. Correlation directions are shown in Figure S9A. R^2 values were computed using the linear regression model.

(B) Inverse correlation between the amount of basal TE transcripts and viral load. The basal TE transcript refers to the proportion of aggregated normalized read counts in TEs among the global transcripts. The black line represents the regression line. R^2 and p values computed using the linear regression model are shown.

(C) Inverse correlation between the basal type I interferon (IFN) signature (score) and viral load. The IFN signature represents the median expression level (TPM value) of genes involved in type I interferon signaling pathways (Table S8).

(D and E) Correlations between the basal expression levels of *SETDB1* (D) and *TRIM28* (E) and viral load. It shows that *SETDB1* (R^2 = 0.42) rather than *TRIM28* (R^2 = 0.03) basal expression is associated with viral load. Basal *SETDB1* expression is also positively correlated with the basal TE transcripts and IFN signature before infection (Figure S9I).

(F) Violin plot of the correlation coefficients between the basal expression of KRAB-ZNFs and other genes with viral load post-infection. A list of human KRAB-ZNFs was obtained from Imbeault et al.[40] and immune genes were obtained from the InnateDB database.[51] The top 10 most correlated KRAB-ZNFs are highlighted.

(G) Violin plot of the correlation coefficients between basal TF expression levels (TPM values) and viral load. Immune and non-immune TFs are compared using the paired Student's t test, and the p value is also shown. Black bars represent mean values. TF genes were obtained from the JASPAR database as we previously used for the motif analysis and Immune TFs were obtained from the InnateDB database. Only expressed TFs are shown. Colors indicate motifs that are enriched in different categories of families, and asterisk highlights the motifs that are enriched in multiple categories.

(H) Multivariable regression model developed for the prediction of viral load using the expression levels of immune TFs in the basal state. The top six correlated TFs to viral load that are also associated with TEs were used. The model was generated as we described in STAR Methods. The formula and variables and adjusted R^2 are shown.

(I) Multivariable regression model developed for the predictive of viral load using the TE-associated non-immune (novel) host factors in the basal state. Using the same approach (see STAR Methods), a subset of features were selected among the age and six non-immune factors, including *SETDB1*, TE transcripts, TE methylation, *ZNF566*, *ZNF611*, and *PLAGL1*.

(J) Multivariable regression model developed for the predictive of viral load using the TE-associated immune and non-immune host factors in the basal state. We included all the non-immune factors as well as *STAT2* to generate the model. *STAT2* was selected on the basis of the correlation to viral load.

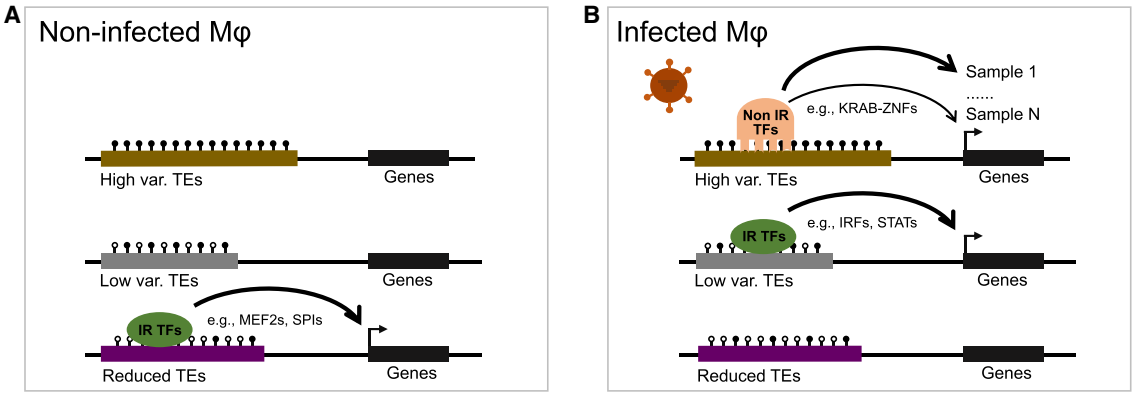

Figure 7. Regulatory models of TEs in response to influenza infection in human primary macrophages

(A) Epigenetic states of enhanced and reduced families in macrophages pre-infection. Before infection, high variable and low variable families are not accessible because of the lack of corresponding TFs binding or repression by high DNA methylation or histone methylation. In contrast, families with reduced accessibility, also called reduced families, are accessible and bound by a distinct set of known immune-related (IR) TFs, including MEF2s and SPIs. High variable families are relatively longer and show a higher DNA and histone methylation level compared with other families.

(B) Epigenetic states of enhanced and reduced families in macrophages post-infection. Chromatin accessibility of high variable and low variable families are enhanced post-infection. High variable families are bound mainly by potential novel host factors (non-IR TFs), including multiple KRAB-ZNFs such as *ZNF566* and *ZNF611*; low variable families are bound mainly by known immune-related regulators (IR TFs), including IRFs and STATs. Reduced TEs are prone to be less accessible because of the decreased expression of various TFs (e.g., MEF2s) post-infection. High variable families display a high variability in accessibility post-infection and may differentially regulate nearby genes between individuals.

we obtained a slightly better fit with a model that includes TE transcripts and the new factors including *ZNF566*, *ZNF611*, and *PLAGL1* (adjusted R^2 = 0.655) (Figure 6I). Adding the top correlated immune TF (i.e., *STAT2*) further increased the accuracy of the model (adjusted R^2 = 0.758) (Figure 6J). As expected, if we used age as an independent variable in these models, the predictive accuracies decreased significantly (Figure S9J). Altogether, we concluded that TEs and TE-related host factors can be used to predict viral load in macrophages post-infection.

DISCUSSION

Inter-individual variability in disease is at the core of precision medicine. By examining TE transcription and epigenetic state in macrophages derived from 39 individuals, we provided new insights into the contribution of TEs to the response to IAV infection. Specifically, we discovered a set of 15 TE families with high inter-individual variability in chromatin accessibility post-infection (Figure 3C). Besides the distinct sequence features and chromatin states they promote, we found that high variable families enrich for TF binding motifs of potentially new host factors in the response to infection (e.g., KRAB-ZNFs); in contrast, other TE families of interest mainly enrich TF binding motifs for known immune regulators (Figures 7, S6, S7). Given that many of the TF binding motifs enriched in high variable families were associated with proteins that are known to interact with the KAP1/TRIM28 machinery suggests that this pathway may contribute to the inter-individual epigenetic variability post-infection. We also speculate that the enhanced accessibility in these families may be because of gradual chromatin de-repression led by the reduced expression of *SETDB1* or *TRIM28* upon infection.

In this study, multiple chromatin regions were identified for each TE family (Figures 5C and 5D). For example, we observed the top peak region of MER44D to be significantly enriched for FOS/JUN related motifs, while another region was enriched mainly for IRF-related motifs. Thus, the same TE family appears to contribute multiple binding regions recognized by different TFs, suggesting that each family may play complex regulatory roles upon infection. Additionally, by comparing the TE enrichment levels between infected and non-infected monocyte-derived macrophages following IAV infection, we were able to identify families with reduced chromatin accessibility (Figure 2F). These families would have been missed by previous approaches that relied on an expected distribution as control.[18,19,47,48] Moreover, although many LINE families were found to have reduced accessibility post-infection, we still observed two LINE families (L1PA12 and L1M2a) with enhanced accessibility. This may be due to the absence in these families of TFBS found enriched in their counterparts with reduced accessibility (e.g., SPIs, MEF2s). On the other hand, the observed epigenetic changes in the LINE families with reduced accessibility may not affect their transcription which were slightly upregulated post-infection.

Our data also revealed a strong inverse correlation between the basal TE transcripts and viral load post-infection. In line with the involvement of TE transcripts in the activation of innate immunity,[26,27] we speculate that TE transcription in macrophages before infection may be involved in the activation of the innate immune response to IAV infection. To further support this claim, we combined TE basal expression levels with other factors identified in the analysis of high variable families, such as TE DNA methylation, *SETDB1*, and *PLAGL1* expression levels, and were able to build a model that was predictive of the response to infection (Figures 6H–6J). Some polymorphic TEs were also found to be expression quantitative trait loci (eQTLs) for genes upon infection, such as *TRIM25*,[49] thus we

speculate that polymorphic TEs may act as enhancers and further contribute to the variable response to infection.

Altogether, our data depict major epigenetic shifts in TEs in human macrophages upon infection, opening mostly in LTR/ERVs and closing in LINEs. It is intriguing to consider that TEs might not only be an important source of regulatory innovation between species[18,19] but also of regulatory variation within a population.

Limitations of the study

The proximity of these variable TE loci to important immune genes suggest that they may contribute to the variable response to influenza infection, although further work will be needed to demonstrate a causal link between variation in TE activity and viral control. Another aspect that would be interesting to dissect is whether the variation observed is consistent over time or a consequence of the fact that we looked at a specific time point. It will also be interesting to expand this analysis and study the contributions of TEs in other immune cells (e.g., $CD4^+$ T cells, pneumocytes, and dendritic cells[5,50]) and to challenges with other pathogens. More samples will be needed to improve and validate the predictive model we constructed using TEs and TE-associated host factors.

STAR★METHODS

Detailed methods are provided in the online version of this paper and include the following:

SUPPLEMENTAL INFORMATION

Supplemental information can be found online at https://doi.org/10.1016/j.xgen.2023.100292.

ACKNOWLEDGMENTS

This work was supported by a Canadian Institutes of Health Research (CIHR) program grant (CEE-151618) for the McGill Epigenomics Mapping Center, which is part of the Canadian Epigenetics, Environment and Health Research Consortium (CEEHRC) Network. G.B. is supported by a Canada Research Chair Tier 1 award, a FRQ-S, Distinguished Research Scholar award, and by the World Premier International Research Center Initiative (WPI), MEXT, Japan. The Canadian Center for Computational Genomics (C3G) is supported by a Genome Canada Genome Technology Platform grant. We would like to acknowledge Calcul Québec and the Digital Research Alliance of Canada for access to computing resources. We thank Drs. Taka Inoue and Erwin Schurr for the helpful discussion and constructive comments.

AUTHOR CONTRIBUTIONS

G.B., L.B., and T.M.P. planned the project and designed the experiments. R.H.M.S., V.Y., A.P., and M.-M.S. performed all experiments in the lab. T.K. provided logistical support. A.S.P. and K.A.A. performed primary data analysis and quality control. S.G., C.G., and Y.L.L. performed some complementary data analyses. X.C. and G.B. designed all analyses presented in this study. X.C. performed the analyses and prepared all figures. X.C. and G.B. wrote the manuscript with the help of L.B. All authors reviewed the final text.

DECLARATION OF INTERESTS

The authors declare no competing interests.

Received: June 14, 2022
Revised: November 15, 2022
Accepted: March 6, 2023
Published: April 7, 2023

REFERENCES

1. Clohisey, S., and Baillie, J.K. (2019). Host susceptibility to severe influenza A virus infection. Crit. Care *23*, 303. https://doi.org/10.1186/s13054-019-2566-7.
2. Fukuyama, S., and Kawaoka, Y. (2011). The pathogenesis of influenza virus infections: the contributions of virus and host factors. Curr. Opin. Immunol. *23*, 481–486. https://doi.org/10.1016/j.coi.2011.07.016.
3. Gounder, A.P., and Boon, A.C.M. (2019). Influenza pathogenesis: the effect of host factors on severity of disease. J. Immunol. *202*, 341–350. https://doi.org/10.4049/jimmunol.1801010.
4. Ciancanelli, M.J., Abel, L., Zhang, S.-Y., and Casanova, J.-L. (2016). Host genetics of severe influenza: from mouse Mx1 to human IRF7. Curr. Opin. Immunol. *38*, 109–120. https://doi.org/10.1016/j.coi.2015.12.002.
5. Iwasaki, A. (2012). A virological view of innate immune recognition. Annu. Rev. Microbiol. *66*, 177–196. https://doi.org/10.1146/annurev-micro-092611-150203.
6. Bierne, H., Hamon, M., and Cossart, P. (2012). Epigenetics and bacterial infections. Cold Spring Harb. Perspect. Med. *2*, a010272. https://doi.org/10.1101/cshperspect.a010272.

7. Paschos, K., and Allday, M.J. (2010). Epigenetic reprogramming of host genes in viral and microbial pathogenesis. Trends Microbiol. *18*, 439–447. https://doi.org/10.1016/j.tim.2010.07.003.

8. Xu, Q., Tang, Y., and Huang, G. (2021). Innate immune responses in RNA viral infection. Front. Med. *15*, 333–346. https://doi.org/10.1007/s11684-020-0776-7.

9. Smale, S.T. (2012). Transcriptional regulation in the innate immune system. Curr. Opin. Immunol. *24*, 51–57. https://doi.org/10.1016/j.coi.2011.12.008.

10. Zhang, Q., and Cao, X. (2021). Epigenetic remodeling in innate immunity and inflammation. Annu. Rev. Immunol. *39*, 279–311. https://doi.org/10.1146/annurev-immunol-093019-123619.

11. Keenan, C.R., and Allan, R.S. (2019). Epigenomic drivers of immune dysfunction in aging. Aging Cell *18*, e12878. https://doi.org/10.1111/acel.12878.

12. Bourque, G. (2009). Transposable elements in gene regulation and in the evolution of vertebrate genomes. Curr. Opin. Genet. Dev. *19*, 607–612. https://doi.org/10.1016/j.gde.2009.10.013.

13. Bourque, G., Burns, K.H., Gehring, M., Gorbunova, V., Seluanov, A., Hammell, M., Imbeault, M., Izsvák, Z., Levin, H.L., Macfarlan, T.S., et al. (2018). Ten things you should know about transposable elements. Genome Biol. *19*, 199. https://doi.org/10.1186/s13059-018-1577-z.

14. Chuong, E.B., Elde, N.C., and Feschotte, C. (2017). Regulatory activities of transposable elements: from conflicts to benefits. Nat. Rev. Genet. *18*, 71–86. https://doi.org/10.1038/nrg.2016.139.

15. Buttler, C.A., and Chuong, E.B. (2022). Emerging roles for endogenous retroviruses in immune epigenetic regulation. Immunol. Rev. *305*, 165–178. https://doi.org/10.1111/imr.13042.

16. Kassiotis, G., and Stoye, J.P. (2016). Immune responses to endogenous retroelements: taking the bad with the good. Nat. Rev. Immunol. *16*, 207–219. https://doi.org/10.1038/nri.2016.27.

17. Srinivasachar Badarinarayan, S., and Sauter, D. (2021). Switching sides: how endogenous retroviruses protect us from viral infections. J. Virol. *95*, e02299-20. https://doi.org/10.1128/JVI.02299-20.

18. Bogdan, L., Barreiro, L., and Bourque, G. (2020). Transposable elements have contributed human regulatory regions that are activated upon bacterial infection. Philos. Trans. R. Soc. Lond. B Biol. Sci. *375*, 20190332. https://doi.org/10.1098/rstb.2019.0332.

19. Chuong, E.B., Elde, N.C., and Feschotte, C. (2016). Regulatory evolution of innate immunity through co-option of endogenous retroviruses. Science *351*, 1083–1087. https://doi.org/10.1126/science.aad5497.

20. Macchietto, M.G., Langlois, R.A., and Shen, S.S. (2020). Virus-induced transposable element expression up-regulation in human and mouse host cells. Life Sci. Alliance *3*, e201900536. https://doi.org/10.26508/lsa.201900536.

21. Mikhalkevich, N., O'Carroll, I.P., Tkavc, R., Lund, K., Sukumar, G., Dalgard, C.L., Johnson, K.R., Li, W., Wang, T., Nath, A., and Iordanskiy, S. (2021). Response of human macrophages to gamma radiation is mediated via expression of endogenous retroviruses. PLoS Pathog. *17*, e1009305. https://doi.org/10.1371/journal.ppat.1009305.

22. Nellåker, C., Yao, Y., Jones-Brando, L., Mallet, F., Yolken, R.H., and Karlsson, H. (2006). Transactivation of elements in the human endogenous retrovirus W family by viral infection. Retrovirology *3*, 44. https://doi.org/10.1186/1742-4690-3-44.

23. Schmidt, N., Domingues, P., Golebiowski, F., Patzina, C., Tatham, M.H., Hay, R.T., and Hale, B.G. (2019). An influenza virus-triggered SUMO switch orchestrates co-opted endogenous retroviruses to stimulate host antiviral immunity. Proc. Natl. Acad. Sci. USA *116*, 17399–17408. https://doi.org/10.1073/pnas.1907031116.

24. Wang, M., Qiu, Y., Liu, H., Liang, B., Fan, B., Zhou, X., and Liu, D. (2020). Transcription profile of human endogenous retroviruses in response to dengue virus serotype 2 infection. Virology *544*, 21–30. https://doi.org/10.1016/j.virol.2020.01.014.

25. Cuellar, T.L., Herzner, A.-M., Zhang, X., Goyal, Y., Watanabe, C., Friedman, B.A., Janakiraman, V., Durinck, S., Stinson, J., Arnott, D., et al. (2017). Silencing of retrotransposons by SETDB1 inhibits the interferon response in acute myeloid leukemia. J. Cell Biol. *216*, 3535–3549. https://doi.org/10.1083/jcb.201612160.

26. Gázquez-Gutiérrez, A., Witteveldt, J., R Heras, S., and Macias, S. (2021). Sensing of transposable elements by the antiviral innate immune system. RNA *27*, 735–752. https://doi.org/10.1261/rna.078721.121.

27. Hale, B.G. (2022). Antiviral immunity triggered by infection-induced host transposable elements. Curr. Opin. Virol. *52*, 211–216. https://doi.org/10.1016/j.coviro.2021.12.006.

28. Bogu, G.K., Reverter, F., Marti-Renom, M.A., Snyder, M.P., and Guigó, R. (2019). Atlas of transcriptionally active transposable elements in human adult tissues. Preprint at bioRxiv. https://doi.org/10.1101/714212.

29. Gorbunova, V., Seluanov, A., Mita, P., McKerrow, W., Fenyö, D., Boeke, J.D., Linker, S.B., Gage, F.H., Kreiling, J.A., Petrashen, A.P., et al. (2021). The role of retrotransposable elements in ageing and age-associated diseases. Nature *596*, 43–53. https://doi.org/10.1038/s41586-021-03542-y.

30. LaRocca, T.J., Cavalier, A.N., and Wahl, D. (2020). Repetitive elements as a transcriptomic marker of aging: evidence in multiple datasets and models. Aging Cell *19*, e13167. https://doi.org/10.1111/acel.13167.

31. Lima-Junior, D.S., Krishnamurthy, S.R., Bouladoux, N., Collins, N., Han, S.-J., Chen, E.Y., Constantinides, M.G., Link, V.M., Lim, A.I., Enamorado, M., et al. (2021). Endogenous retroviruses promote homeostatic and inflammatory responses to the microbiota. Cell *184*, 3794–3811.e19. https://doi.org/10.1016/j.cell.2021.05.020.

32. Aracena, K.A., Lin, Y.-L., Luo, K., Pacis, A., Gona, S., Mu, Z., Yotova, V., Sindeaux, R., Pramatarova, A., Simon, M.-M., et al. (2022). Epigenetic variation impacts ancestry-associated differences in the transcriptional response to influenza infection. Preprint at bioRxiv. https://doi.org/10.1101/2022.05.10.491413.

33. Granados, A., Peci, A., McGeer, A., and Gubbay, J.B. (2017). Influenza and rhinovirus viral load and disease severity in upper respiratory tract infections. J. Clin. Virol. *86*, 14–19. https://doi.org/10.1016/j.jcv.2016.11.008.

34. de Jong, M.D., Simmons, C.P., Thanh, T.T., Hien, V.M., Smith, G.J.D., Chau, T.N.B., Hoang, D.M., Chau, N.V.V., Khanh, T.H., Dong, V.C., et al. (2006). Fatal outcome of human influenza A (H5N1) is associated with high viral load and hypercytokinemia. Nat. Med. *12*, 1203–1207. https://doi.org/10.1038/nm1477.

35. Li, C.-C., Wang, L., Eng, H.-L., You, H.-L., Chang, L.-S., Tang, K.-S., Lin, Y.-J., Kuo, H.-C., Lee, I.-K., Liu, J.-W., et al. (2010). Correlation of pandemic (H1N1) 2009 viral load with disease severity and prolonged viral shedding in children - volume 16, number 8—august 2010 - emerging infectious diseases. Emerg. Infect. Dis. *16*, 1265–1272. https://doi.org/10.3201/eid1608.091918.

36. Thorburn, F., Bennett, S., Modha, S., Murdoch, D., Gunson, R., and Murcia, P.R. (2015). The use of next generation sequencing in the diagnosis and typing of respiratory infections. J. Clin. Virol. *69*, 96–100. https://doi.org/10.1016/j.jcv.2015.06.082.

37. O'Neill, M.B., Quach, H., Pothlichet, J., Aquino, Y., Bisiaux, A., Zidane, N., Deschamps, M., Libri, V., Hasan, M., Zhang, S.-Y., et al. (2021). Single-cell and bulk RNA-sequencing reveal differences in monocyte susceptibility to influenza A virus infection between africans and Europeans. Front. Immunol. *12*, 768189. https://doi.org/10.3389/fimmu.2021.768189.

38. Tretina, K., Park, E.-S., Maminska, A., and MacMicking, J.D. (2019). Interferon-induced guanylate-binding proteins: guardians of host defense in health and disease. J. Exp. Med. *216*, 482–500. https://doi.org/10.1084/jem.20182031.

39. Srinivasachar Badarinarayan, S., Shcherbakova, I., Langer, S., Koepke, L., Preising, A., Hotter, D., Kirchhoff, F., Sparrer, K.M.J., Schotta, G., and Sauter, D. (2020). HIV-1 infection activates endogenous retroviral promoters regulating antiviral gene expression. Nucleic Acids Res. *48*, 10890–10908. https://doi.org/10.1093/nar/gkaa832.

40. Imbeault, M., Helleboid, P.-Y., and Trono, D. (2017). KRAB zinc-finger proteins contribute to the evolution of gene regulatory networks. Nature *543*, 550–554. https://doi.org/10.1038/nature21683.

41. Barazandeh, M., Lambert, S.A., Albu, M., and Hughes, T.R. (2018). Comparison of ChIP-seq data and a reference motif set for human KRAB C2H2 zinc finger proteins. G3 *8*, 219–229. https://doi.org/10.1534/g3.117.300296.

42. Helleboid, P.-Y., Heusel, M., Duc, J., Piot, C., Thorball, C.W., Coluccio, A., Pontis, J., Imbeault, M., Turelli, P., Aebersold, R., and Trono, D. (2019). The interactome of KRAB zinc finger proteins reveals the evolutionary history of their functional diversification. EMBO J. *38*, e101220. https://doi.org/10.15252/embj.2018101220.

43. Iyengar, S., and Farnham, P.J. (2011). KAP1 protein: an enigmatic master regulator of the genome. J. Biol. Chem. *286*, 26267–26276. https://doi.org/10.1074/jbc.R111.252569.

44. Potthoff, M.J., and Olson, E.N. (2007). MEF2: a central regulator of diverse developmental programs. Development *134*, 4131–4140. https://doi.org/10.1242/dev.008367.

45. Clark, R.I., Tan, S.W.S., Péan, C.B., Roostalu, U., Vivancos, V., Bronda, K., Pilátová, M., Fu, J., Walker, D.W., Berdeaux, R., et al. (2013). MEF2 is an in vivo immune-metabolic switch. Cell *155*, 435–447. https://doi.org/10.1016/j.cell.2013.09.007.

46. Van Dyck, F., Delvaux, E.L.D., Van de Ven, W.J.M., and Chavez, M.V. (2004). Repression of the transactivating capacity of the oncoprotein PLAG1 by SUMOylation. J. Biol. Chem. *279*, 36121–36131. https://doi.org/10.1074/jbc.M401753200.

47. Ito, J., Sugimoto, R., Nakaoka, H., Yamada, S., Kimura, T., Hayano, T., and Inoue, I. (2017). Systematic identification and characterization of regulatory elements derived from human endogenous retroviruses. PLoS Genet. *13*, e1006883. https://doi.org/10.1371/journal.pgen.1006883.

48. Sakashita, A., Maezawa, S., Takahashi, K., Alavattam, K.G., Yukawa, M., Hu, Y.-C., Kojima, S., Parrish, N.F., Barski, A., Pavlicev, M., and Namekawa, S.H. (2020). Endogenous retroviruses drive species-specific germline transcriptomes in mammals. Nat. Struct. Mol. Biol. *27*, 967–977. https://doi.org/10.1038/s41594-020-0487-4.

49. Groza, C., Chen, X., Pacis, A., Simon, M.-M., Pramatarova, A., Aracena, K.A., Pastinen, T., Barreiro, L.B., and Bourque, G. (2021). Genome graphs detect human polymorphisms in active epigenomic states during influenza infection. Preprint at bioRxiv. https://doi.org/10.1101/2021.09.29.462206.

50. Marasca, F., Sinha, S., Vadalà, R., Polimeni, B., Ranzani, V., Paraboschi, E.M., Burattin, F.V., Ghilotti, M., Crosti, M., Negri, M.L., et al. (2022). LINE1 are spliced in non-canonical transcript variants to regulate T cell quiescence and exhaustion. Nat. Genet. *54*, 180–193. https://doi.org/10.1038/s41588-021-00989-7.

51. Breuer, K., Foroushani, A.K., Laird, M.R., Chen, C., Sribnaia, A., Lo, R., Winsor, G.L., Hancock, R.E.W., Brinkman, F.S.L., and Lynn, D.J. (2013). InnateDB: systems biology of innate immunity and beyond—recent updates and continuing curation. Nucleic Acids Res. *41*, D1228–D1233. https://doi.org/10.1093/nar/gks1147.

52. Bolger, A.M., Lohse, M., and Usadel, B. (2014). Trimmomatic: a flexible trimmer for Illumina sequence data. Bioinformatics *30*, 2114–2120. https://doi.org/10.1093/bioinformatics/btu170.

53. Kim, D., Pertea, G., Trapnell, C., Pimentel, H., Kelley, R., and Salzberg, S.L. (2013). TopHat2: accurate alignment of transcriptomes in the presence of insertions, deletions and gene fusions. Genome Biol. *14*, R36. https://doi.org/10.1186/gb-2013-14-4-r36.

54. Li, H., Handsaker, B., Wysoker, A., Fennell, T., Ruan, J., Homer, N., Marth, G., Abecasis, G., and Durbin, R.; 1000 Genome Project Data Processing Subgroup (2009). The sequence alignment/map format and SAMtools. Bioinformatics *25*, 2078–2079. https://doi.org/10.1093/bioinformatics/btp352.

55. Edwards, J.A., and Edwards, R.A. (2019). Fastq-pair: efficient synchronization of paired-end fastq files. Preprint at bioRxiv552885. https://doi.org/10.1101/552885.

56. Jin, Y., Tam, O.H., Paniagua, E., and Hammell, M. (2015). TEtranscripts: a package for including transposable elements in differential expression analysis of RNA-seq datasets. Bioinformatics *31*, 3593–3599. https://doi.org/10.1093/bioinformatics/btv422.

57. Love, M.I., Huber, W., and Anders, S. (2014). Moderated estimation of fold change and dispersion for RNA-seq data with DESeq2. Genome Biol. *15*, 550. https://doi.org/10.1186/s13059-014-0550-8.

58. Raudvere, U., Kolberg, L., Kuzmin, I., Arak, T., Adler, P., Peterson, H., and Vilo, J. (2019). g:Profiler: a web server for functional enrichment analysis and conversions of gene lists (2019 update). Nucleic Acids Res. *47*, W191–W198. https://doi.org/10.1093/nar/gkz369.

59. Quinlan, A.R., and Hall, I.M. (2010). BEDTools: a flexible suite of utilities for comparing genomic features. Bioinformatics *26*, 841–842. https://doi.org/10.1093/bioinformatics/btq033.

60. Bailey, T.L., Boden, M., Buske, F.A., Frith, M., Grant, C.E., Clementi, L., Ren, J., Li, W.W., and Noble, W.S. (2009). MEME Suite: tools for motif discovery and searching. Nucleic Acids Res. *37*, W202–W208. https://doi.org/10.1093/nar/gkp335.

61. Fornes, O., Castro-Mondragon, J.A., Khan, A., van der Lee, R., Zhang, X., Richmond, P.A., Modi, B.P., Correard, S., Gheorghe, M., Baranašić, D., et al. (2020). Jaspar 2020: update of the open-access database of transcription factor binding profiles. Nucleic Acids Res. *48*, D87–D92. https://doi.org/10.1093/nar/gkz1001.

62. Bourque, G., Leong, B., Vega, V.B., Chen, X., Lee, Y.L., Srinivasan, K.G., Chew, J.-L., Ruan, Y., Wei, C.-L., Ng, H.H., and Liu, E.T. (2008). Evolution of the mammalian transcription factor binding repertoire via transposable elements. Genome Res. *18*, 1752–1762. https://doi.org/10.1101/gr.080663.108.

63. Lander, E.S., Linton, L.M., Birren, B., Nusbaum, C., Zody, M.C., Baldwin, J., Devon, K., Dewar, K., Doyle, M., FitzHugh, W., et al. (2001). Initial sequencing and analysis of the human genome. Nature *409*, 860–921. https://doi.org/10.1038/35057062.

STAR★METHODS

KEY RESOURCES TABLE

REAGENT or RESOURCE	SOURCE	IDENTIFIER
Biological samples		
Macrophage	Aracena et al.[32]	N/A
Deposited data		
RNAseq and ATACseq and ChiP-seq	Aracena et al.[32]	EGAD00001008422
WGBS	Aracena et al.[32]	EGAD00001008359
KAP1 and KRAB-ZNF ChiP-seq	Imbeault et al.[40]	GSE78099
Software and algorithms		
VariabilityInTE	This Study	https://github.com/xunchen85/VariabilityInTEs; Zenodo https://doi.org/10.5281/zenodo.7532781
Trimmomatic version 0.36	Bolger et al.[52]	http://www.usadellab.org/cms/?page=trimmomatic
TopHat2 version 2.1.1	Kim et al.[53]	https://ccb.jhu.edu/software/tophat
SAMtools version 1.10	Li et al.[54]	https://github.com/samtools/samtools
Fastq-pair version 0.3	Edwards et al.[55]	https://github.com/linsalrob/fastq-pair
Tetranscripts version 2.1.4	Jin et al.[56]	https://github.com/mhammell-laboratory/Tetranscripts
DESeq2 version 1.32.0	Love et al.[57]	https://bioconductor.org/packages/release/bioc/html/DESeq2.html
PCAtools version 2.4.0	N/A	https://github.com/kevinblighe/PCAtools
g:Profiler	Raudvere et al.[58]	https://biit.cs.ut.ee/gprofiler/gost
BEDtools version 2.30.0	Quinlan et al.[59]	https://github.com/arq5x/bedtools2
MEME version 5.0.3	Bailey et al.[60]	https://meme-suite.org/meme/doc/download.html
R version 4.1.0	N/A	https://www.r-project.org
Python version 3.7.7	N/A	https://www.python.org
mysql version 5.7	N/A	https://www.mysql.com
ggplot2 version 3.3.5	N/A	https://ggplot2.tidyverse.org
heatmap.2 version 3.1.1	N/A	https://www.rdocumentation.org/packages/gplots/versions/3.1.1
immuneTE	Bogdan et al.[18]	https://github.com/lubogdan/ImmuneTE
JASPAR 2020	Fornes et al.[61]	https://jaspar2020.genereg.net/download/data/2020/CORE/JASPAR2020_CORE_non-redundant_pfms_meme.txt
KRAB-ZNF motif database	Barazandeh et al.[41]	http://kznfmotifs.ccbr.utoronto.ca/data.html
InnateDB version 5.4	Breuer et al.[51]	https://www.innatedb.com/

RESOURCE AVAILABILITY

Lead contact

Further information and request for resources and reagents should be directed to and will be fulfilled by the lead contact, Guillaume Bourque (guil.bourque@mcgill.ca).

Materials availability

This study did not generate new unique reagents.

Data and code availability

- All datasets used in this study have been deposited,[32] and are available at the European Genome-phenome Archive (EGA) as follows: RNA-seq & ATAC-seq & ChIP-seq – EGA: EGAD00001008422; and WGBS – EGA: EGAD00001008359.
- We also constructed a versatile browser (https://computationalgenomics.ca/tools/epivar), which allows users to explore genomic tracks for gene expression, chromatin accessibility, histone modifications, DNA methylation.

- Scripts for main analyses are available at https://github.com/xunchen85/VariabilityInTEs and Zenodo with the linked https://doi.org/10.5281/zenodo.7532781.
- Any additional information required to reanalyze the data reported in this paper is available from the lead contact upon request.

EXPERIMENTAL MODEL AND SUBJECT DETAILS

Materials and sequencing data generation

To study the inter-individual variability in TEs following influenza A (IAV) infection, we collected primary macrophage cells from peripheral blood mononuclear cells of 39 healthy female individuals with African American (n = 19) and European-American (n = 20) ancestry between 18 and 54 years old. We then infected macrophages (cultured for 6 days) with IAV for 24-h and collected both non-infected and infected macrophages for multiple sequencing assays. The details were described here.[32] Briefly, we conducted the ATAC-seq assay to study chromatin accessibility. Using chromatin immunoprecipitation sequencing (ChIP-seq) technology, we also investigated the genome-wide profiles of H3K27ac, H3K4me1, H3K4me3, and H3K27me3 histone modifications. H3K27ac and H3K4me1 have been widely used to mark enhancers; H3K4me3 mark has been associated with promoters or active transcription; H3K27me3 mark has been associated with chromatin repression. Whole-genome bisulfite sequencing (WGBS) was further used to profile genome-wide DNA methylation. RNA sequencing (RNA-seq) was used to profile the transcriptome. All sequencing assays were performed in both infected and non-infected macrophages of each donor. Samples and generated sequencing datasets were summarized in Table S1.[32] Detailed methodologies to profile the genome-wide DNA methylation level and chromatin modifications were also described here.[32]

METHOD DETAILS

RNA-seq read alignment

Trimmomatic (v0.36) was first used to trim adapter sequences with the parameters *PE -phred33 -quiet -validatePairs ILLUMINACLIP*:*$EBROOTTRIMMOMATIC/adapters/TruSeq3-PE.fa*:*2*:*30*:*15*:*2*:*true LEADING*:*3 TRAILING*:*30 MINLEN*:*50*.[52] After trimming off the adapters and low-quality nucleotides, high-quality paired-end RNA-seq reads were aligned against the human reference genome (hg19, https://hgdownload.soe.ucsc.edu/goldenPath/hg19/bigZips/hg19.fa.gz) using TopHat2 v2.1.1.[53] To optimize for the analysis of TE transcription, we kept multi-mapped reads with the recommended parameters *-x 100 –no-mixed*.[56] Gene annotation file "*hg19.ensGene.gtf*" was obtained from https://hgdownload.soe.ucsc.edu/goldenPath/hg19/bigZips/genes/.

Viral load calculation

To estimate the viral load, we re-aligned high-quality paired-end RNA-seq reads against the human reference genome (hg38, https://hgdownload.soe.ucsc.edu/goldenPath/hg38/bigZips/hg38.fa.gz) using TopHat2 with the default parameters. Paired-end unmapped reads were extracted from the unmapped BAM files and converted to FASTQ format using SAMtools (v1.10) *fastq* function.[54] Obtained FASTQ files were then reformatted using Fastq-pair (v0.3) tool with the parameter *-t 1000000*.[55] Using TopHat2 with the same parameters, paired-end unmapped reads were aligned against the influenza A virus (H1N1) reference genome, which contains eight fragments including NC_002016.1, NC_002017.1, NC_002018.1, NC_002019.1, NC_002020.1, NC_002021.1, NC_002022.1, NC_002023.1. After that, we retrieved the number of reads mapped to influenza. Lastly, viral load was computed as the percentage of reads mapped to the influenza genome versus the total number of reads mapped to both human and influenza reference genomes.

Gene/TE expression levels measurement

TEcount implemented by TEtranscripts (v2.1.4)[56] was used to measure the gene and TE expression at the family level using RNA-seq data. Expression of each family represents the total number of reads mapped to all instances from the same family. We ran it with the use of sorted BAM file as the input and following parameters: *–sortByPos –TE hg19_rmsk_TE.gtf –GTF hg19.ensGene.gtf –stranded reverse –mode multi*. The repeat annotation file "*hg19_rmsk_TE.gtf*" was downloaded from http://labshare.cshl.edu/shares/mhammelllab/www-data/TEtranscripts/TE_GTF/. After running, we obtained the output file for each sample which contains two columns, one column specifying the names of genes and TE families, and another column specifying corresponding read counts. The output files of all samples were combined into a count matrix for the downstream analysis.

Differential expression and PCA analysis

To perform the differential expression analysis, the obtained count matrix was used as the input to DESeq2 v3.9.[57] Non-infected samples were used as the control group and infected samples were used as the case group. After the removal of non-expressed TE families and genes (<2 reads across samples), the count matrix was then standardized following QC steps of *DESeqDataSetFromMatrix*, *estimateSizeFactors*, *estimateDispersions*, and *nbinomWaldTest* included by DESeq2. Lastly, after we retrieved the output using the *results* function, we kept the significantly differentially expressed genes and TE families from DNA, LINE, SINE, LTR and SVA subclasses with the thresholds of $|\log2FC| \geq 1$ and adjusted p value ≤ 0.001.

To perform the principal component analysis (PCA), we applied a variance stabilizing transformation (vst) to the achieved normalized count matrix. We then used the PCAtools *pca* function with the parameter *removeVar = 0.1* for the PCA analysis and *biplot* function for the visualization (https://github.com/kevinblighe/PCAtools). Genes and TE families were analyzed separately.

Expression levels normalization

Transcripts per kilobase million (TPM) values were calculated using the raw count matrix for genes and TE families. Specifically, we first computed the reads per kilobase (RPK) for each gene and family. For genes, we divided the read counts by the aggregated total lengths of exons per gene in kilobases; for TE families, we divided the read counts by the aggregated lengths across all instances per family. We next counted up the RPK values of both genes and TE families and divided them by 1,000,000 to obtain the TPM values.

Genes and viral load correlation analysis

We then examined which differentially expressed genes (DEGs) are correlated with viral load. Here, we only considered highly-expressed genes with an average of TPM values ≥ 1 in either infected or non-infected samples. The expression fold change (log2FC) of each gene was computed using the formula: $log\ 2\ FC = log\ 2(TPM^{Flu} + 0.01) - log\ 2(TPM^{NI} + 0.01)$. FCs were correlated with viral load post-infection using R *lm* function. DEGs correlated with viral load ($R^2 \geq 0.3$ and p value ≤ 0.05) were then submitted to the g:Profiler (https://biit.cs.ut.ee/gprofiler/gost) with the default parameters for the pathway enrichment analysis.[58] G:SCS threshold with a minimum p value of 0.05 was used to determine the enriched pathways. Kyoto Encyclopedia of Genes and Genomes (KEGG) database was used to determine the enriched pathways and the top 30 terms were visualized. Key immune regulators involved in the RNA viral signaling pathway were obtained here.[8] Similarly, we also correlated the basal gene expression (TPM) with viral load.

TEs and viral load correlation analysis

To measure the variability of TE transcription, we correlated expression fold changes of each family with viral load post-infection. Expression FC of each family per sample was computed with the same formula: $log2FC = log\ 2(TPM^{Flu} + 0.01) - log\ 2(TPM^{NI} + 0.01)$. Similarly, R *lm* function was used for the correlation analyses. Positive and negative correlated ($R^2 \geq 0.3$ and p value ≤ 0.05) families were reported.

To study the enrichment of positively or negatively associated families among each TE subclass, we performed the permutation test by comparing the actual proportion of positively/negatively correlated families among each TE subclass or superfamily relative to 10,000 randomized proportions. *p* value was calculated using the formula in R: $P\ value = 2 \times mean(randomized\ counts \geq actual\ counts)$.

Using the same approach, we correlated the expression of TE families in infected and non-infected samples with viral load post-infection. Computed TPM values were used for the correlation analysis.

Peaks-associated TEs detection

After profiling the epigenetic state, we obtained ATAC-seq and Chip-seq narrow peaks in BED format. Peak regions were then converted to peak summits (median positions). To identify ATAC-seq peaks-associated instances, peak summits were intersected with the obtained repeat annotation file "hg19_rmsk_TE.gtf" using BEDtools v2.29.2 *intersect* function[59] with the parameters *-wa -u*. The same analysis was performed for other histone marks.

Epigenetic variability analysis

Unique ATAC-seq consensus peaks were obtained as we previously described.[32] To identify consensus peaks in TEs, we first converted peak regions to summits (median positions) and then intersected with the repeat annotation file aforementioned using BEDtools *intersect* function with the parameters *-wa -wb*. After that, read counts were normalized to RPM value for the downstream comparative analysis across samples. Specifically, the read count was first divided by the total number of reads and then multiplied 1,000,000. The coefficient of variation (*cv*) of each peak region was computed using the formula: $cv = \left|\frac{\text{standard deviation}}{\text{mean}}\right|$. Infected and non-infected samples were analyzed separately. Consensus peak regions with a minimum RPM value of "1" were kept. Variable regions were defined as the peak regions with *cv* values ≥ 0.5, referring to regions with the standard deviation that is half of the mean. Proportions of variable regions in TEs and non-TEs were compared. Same analysis was performed for other histone marks.

TEs with epigenetic changes detection

We next aimed to identify TE families with enhanced accessibility upon infection. Firstly, we normalized the number of peaks-associated instances per family. Briefly, we divided the number of peaks-associated instances by the total number of peaks per sample, and then multiplied the average number of peaks across samples. Infected and non-infected samples were normalized, separately. Secondly, to identify families with enhanced accessibility during infection, we kept families with significantly more peaks-associated instances (≥ 1.5-fold, adjusted p value ≤ 0.05) in infected than non-infected samples. Two-tailed paired Student's *t* test was used for the comparison and the resulting p value was adjusted for multiple testing with the Benjamini-Hochberg using the R *p.adjust* function. Lastly, we kept family candidates from DNA, LINE, SINE, LTR, and SVA subclasses with a minimum of 20 peaks-associated instances on average among either infected or non-infected samples.

Similarly, to identify families with reduced accessibility, we kept families with significantly more peaks-associated instances ($\geq$1.5-fold, adjusted p value $\leq$0.05) in non-infected than infected samples. Same analysis was applied to each histone mark to identify families with dynamic regulatory (e.g., enhancer or promoter) potentials upon infection.

We also computed the enrichment level of each family by comparing the actual number of peaks-associated instances with its expected distribution.[18] Specifically, we first annotated peaks-associated instances using BEDtools *intersect* function with the parameters *-wa -u* based on the annotation files (i.e., desert, distal, proximal, 5′ untranslated region (5′UTR), promoter, transcription start site (TSS), exon, and intron regions) obtained from https://github.com/lubogdan/ImmuneTE. We then shuffled the true peaks while keeping the distribution relative to each region using BEDtools *shuffle* function with the parameters *-incl* or *-excl*, for 1000 times. The randomized peaks were intersected with the repeat annotation file to achieve the number of expected peaks-associated instances per family. Lastly, we computed the enrichment level of each family as the actual number of peaks-associated instances relative to the average number of the expected values.

TE clustering analysis

To identify families with high variability, we performed the semi-supervised clustering analysis of enhanced families in 35 infected samples. Here, to rule out the impacts of different genomic distribution between TE families, we used the enrichment level relative to the expected distribution rather than the actual number of instances for the clustering analysis. Briefly, the enrichment levels of enhanced families were gathered into a data matrix followed by the log2 conversion. R *heatmap.2* function was used to perform the unsupervised clustering analysis with the default parameters. Based on the obtained enrichment pattern among samples, we re-ordered the families. Families with higher enrichment levels in Group 3 individuals than Group 1 individuals were distinguished. Non-infected samples were analyzed separately.

We then want to understand whether individual instances from high variable families display a high variability in infected samples. Peaks-associated instances from high variable families were collected. Instances with open chromatin were recorded as "1"; instances with closed chromatin were recorded as "0". We then performed the clustering analysis using R *hclust* function with the default parameters.

High variable instances analysis

For each accessible instance, we first computed the percentage of samples from each group that were accessible post-infection. Next, we defined commonly accessible instances as the instances that were accessible in 25% or more samples from one individual group; we also defined rarely accessible instances as the instances that were accessible in less than 25% samples from any groups. An instance that was accessible in more than 25% samples for commonly accessible instances and one or more samples for rarely accessible instances was considered as enriched in one individual group. Lastly, we computed the proportion of instances that were prone to be accessible in each group.

TE age estimation

The evolutionary age of each instance was estimated using our previous approach.[18,62] In brief, the sequence divergence of each instance relative to the corresponding consensus sequence was obtained from the ".align" file generated by RepeatMasker (https://www.repeatmasker.org/). Hg19 ".align" file was obtained from the UCSC database (https://hgdownload.soe.ucsc.edu/goldenPath/hg19/bigZips/). The divergence rate of each instance was divided by the substitution rate for the human genome (2.2×10^{-9}) to compute the age per instance.[63] The average ages across all instances was referred to the age of each TE family.

TE peak centroids detection

We next want to fine-map the peak centroid on each accessible instance. Read depths were extracted from the aligned BAM file using BEDtools *genomecov* function with the parameter *-d* and then divided by 1,000,000 to compute the RPM values. We then aggregated (summed) RPM values of each nucleotide across accessible instances. Infected and non-infected samples were analyzed separately. The nucleotide with the highest RPM value was recorded as the peak centroid of each instance. Peak centroids in infected samples were used for families with enhanced accessibility; peak centroids in non-infected samples were used for families with reduced accessibility.

Alignment of instances to consensus sequences

We next wanted to map accessible instances to corresponding consensus sequences. The aforementioned RepeatMasker ".align" file was used to retrieve the consensus positions at single-nucleotide resolution. Instances with consistent start and end positions with the ".out" file were kept for downstream analyses. The inconsistency was potentially due to the defective annotation methodologies for the nested instances, extremely short instances, etc. It was a fact that instances of one TE family may be aligned to different consensus sequences. Thus, we wanted to focus on instances aligned to the most representative consensus sequence for each family. In the end, we pinpointed the peak centroid to the consensus sequence.

We plotted the aggregated RPM values relative to the consensus sequence using R. We also clustered accessible instances using the RPM values relative to the consensus sequence. Specifically, after *z*-transformation, scaled RPM values $\leq$0 and consensus

regions with deletions were recoded as "0". R function *heatmap.2* with the default parameter was used for the unsupervised clustering analysis. Heatmap was plotted using *ggplot2* in R.

TE peak regions detection

We next wanted to identify "TE peak regions", which referred to the consensus regions that become accessible on multiple instances. We first excluded instances that were only accessible in the outlier sample and then used the sliding window approach to identify TE peak regions. To iterate over the entire consensus sequence, the window size was set at 100 bp with a step size of one base pair. In each step, we counted the total number of peak centroids within each 100 bp window. The 100 bp-window containing the most peak centroids was identified as a TE peak region ($\geq$5 peak centroids). After the exclusion of previously counted peak centroids, the analysis was repeated until all candidate TE peak regions were identified. The proportion of instances in each TE peak region was computed. TE peak regions were identified using peak centroids in infected samples for enhanced families and non-infected samples for reduced families.

Motif enrichment analysis

Firstly, we extracted 100 bp sequence centered at the centroid of each TE instance using BEDtools *getfasta* function with the *-s* parameter and then used the MEME *fimo* function to search the extracted sequences for known motifs from the latest eighth release of JASPAR motif database (http://jaspar.genereg.net/download/CORE/JASPAR2020_CORE_vertebrates_non-redundant_pfms_meme.txt).[60,61] Instances uniquely accessible in the outlier sample were excluded. Secondly, instances were categorized into each TE peak region, e.g., TE peak region with the most instances was named as "Region 1" and so on. TE peak regions with less than five instances were excluded. Instances not in TE peak regions were grouped as "No regions". Thirdly, we computed the proportion of instances (100 bp centered at the centroid) containing each motif for each TE peak region. The top 5 most abundant motifs in each TE peak region were kept as candidates. To obtain enriched motifs per family, we kept motif candidates appearing in more than 20% instances in each TE peak region and more than 50% instances per family. Lastly, the same motifs detected in multiple TE peak regions were aggregated (summed) to recalculate the proportion; motifs enriched in a total of $\geq$50 instances across families were kept as top candidates. After the analysis, enriched motifs were compared between different TE peak regions and families.

The JASPAR motif database contains a small number (<30) of KRAB-ZNF motifs. To comprehensively search for KRAB-ZNF motifs in TEs, we further screened motifs across the accessible TE instances from enhanced families by using the 242 KRAB-ZNF motifs reported by Barazandeh et al.[41]

KRAB-ZNF binding site enrichment analysis

To explore whether KRAB-ZNF binding sites are enriched in enhanced families, we achieved the KRAB-ZNF binding sites reported by Imbeault et al.[40] We then computed the enrichment level of KAP1 and each KRAB-ZNF across TE families using the same approach as we described above.

We also inspected whether the KAP1 and KRAB-ZNFs are in the open chromatin regions in TEs. To do it, we first extracted 100 bp centered at the ATAC-seq peak centroid of each TE instance in BED format. Then, the extracted 100-bp open chromatin regions in flu samples were intersected with KRAB-ZNF binding sites using BEDtools *intersect* function with the parameters *-wa -wb -f 0.5 -F 0.5 -e -a*. Candidate KRAB-ZNFs that are located in the open chromatin regions of a minimum of 5% accessible instances from any enhanced families were kept.

We further looked at the expression of KRAB-ZNFs that are associated with high variable families in infected samples. To do it, we first achieved the number of reads mapped to each accessible instance using BEDtools *coverage* function with the TE annotation file and parameter "*-counts*". After we obtained the RPKM value per instance (reads per kilobase per million mapped reads), all accessible instances from a family were aggregated as the representative of the accessibility of each family. We then performed the correlative analysis between each high variable family and the expression levels of KRAB-ZNFs using R *lm* function, respectively. Strongly correlated KRAB-ZNFs with any high variable families ($R^2 \geq 0.3$ and p value $\leq$0.05) were kept.

TE regulation of neighboring genes

To explore whether TEs regulate neighboring genes, we examined differentially expressed genes (DEGs) nearby flu-specific instances from enhanced families and nearby NI-specific instances from reduced families. After the differential expression analysis, we retrieved corresponding gene names and coordinates through the command line and parameters: *mysql –user=genome -N –host=genome-mysql.cse.ucsc.edu -A -D hg19 -e "select ensGene.name, name2, chrom, strand, txStart, txEnd, value from ensGene, ensemblToGeneName where ensGene.name = ensemblToGeneName.name"*. To compute the distance between genes and TEs, the first nucleotide (5′ end) (TSS) was used to represent each gene and the median position was used to represent each TE instance. Highly expressed genes (average TPM values $\geq$1 in either infected or non-infected samples) were used for the analysis. BEDtools *window* function was used to obtain human genes centered at each accessible instance within an 1-Mb window. We then computed the proportion of significantly upregulated and downregulated genes among inspected genes, respectively, within each interval of 0-50 kb, 50–100 kb, 100–200 kb, 200–300 kb and so on. Each gene was counted once within each interval.

We also compared the proportions of significantly up/down regulated genes with the expected distribution to compute the statistical significance. Accessible instances were randomly shuffled for high variable, low variable families, and reduced families for 1000 times separately. After the detection of genes near accessible instances, the proportions of significantly up/down regulated genes were computed as the expected values. The binomial distribution of the proportions of up/down regulated genes within each genomic interval was plotted with the 95% confidence interval, suggesting a statistical significance of $p < 0.05$ for any observed values outside the distribution. We then compared the proportions of significantly up/down regulated genes near accessible instances from high variable families, low variable families, and families with reduced accessibility.

We also compared the proportion of up/down regulated genes between flu-specific, NI-specific instances and instances overlapped with shared peaks (instances that were accessible in both infected and non-infected samples).

To identify genes that are potentially regulated by nearby TE-loci, we first picked TE instances overlapped with ATAC-seq peak centroids. We then intersected these instances with the consensus peak regions of ATAC-seq, H3K27ac and H3K4me1 peaks[32] using BEDtools2 *intersect* function with the parameters *-wa -wb -f 0.5 -F 0.5 -e -a*. Candidate TE-loci with significant changes of both ATAC-seq and active marks (H3K27ac and/or H3K4me1) were kept. We lastly obtained significantly up-regulated genes near ($\leq$50 kb) repeat loci from enhanced families and downregulated genes near reduced families. Correlation analysis was also performed using R *lm* function between the TE accessibility and nearby gene expression level post infection.

Profile of DNA methylation and histone marks

Focusing on enhanced families, we calculated the number and proportion of accessible instances overlapped with each mark post-infection. Specifically, we used BEDtools *intersect* function to identify accessible instances overlapped with each histone mark in infected samples. The median position of each peak was used for the analysis. We further identified instances overlapped with both H3K27ac and H3K4me1 marks in infected samples, suggesting the active or strong enhancer potential. We also computed the number and proportion of nearby DEGs within 100 kb (log2FC $\geq$ 0.5, adjusted p value $\leq$0.05). Additionally, we computed the average DNA methylation level of each instance and then we used the mean value across instances to represent the DNA methylation level of the family. DNA methylation level was calculated as the number of methylated cytosines divided by the sum of methylated and unmethylated cytosines at each locus.

Pathway enrichment analysis

The list of significantly up/down regulated genes near each accessible instance was obtained using BEDtools *window* function with the parameters *-l 100000 -r 100000*. The transcription start site was used to represent each gene. We focused on the significantly upregulated genes near accessible instances (within 50 kb) for high variable and low variable families, and significantly downregulated genes near accessible instances for reduced families. The obtained gene lists were submitted to the g:profiler tool with the same settings for the pathway enrichment analysis. We visualized the enriched pathways using *ggplot2* in R.

Global TE transcripts calculation

The amount of global TE transcripts was computed as the proportion of aggregated (summed) read counts normalized by DEseq2 in TEs among the total RNA-seq read counts in both TEs and genes. The linear regression model was used to evaluate the correlation between the basal TE transcripts and viral load post-infection. R *lm* function was used for the analysis and the corresponding p value and R^2 were reported. Using the same approach, we further analyzed each of the four main TE subclasses, i.e., DNA, LINE, SINE and LTR.

Average DNA methylation levels calculation

We computed the average DNA methylation levels among examined CpG sites across all annotated TE regions (TE methylation) in non-infected samples. TE families from the four main subclasses were considered.

Predictive models construction

Multiple regression analysis was used to build the predictive models. Viral load post-infection was used as the outcome of the models. The baseline of IFN signature (score) was computed as the median TPM value amongst 39 expressed genes from type I IFN signaling pathways (Table S8). We first included the baseline of IFN signature and age as predictive variables. We then chose the top six correlated immune TFs of which basal expression levels are also associated with TEs as variables, including *STAT2*, *IRF1*, *IRF7*, *IRF9*, *STAT5A*, and *REL*. We also picked non-immune factors that were associated with TEs as predictive variables, including age, the basal amount of TE transcripts, the average DNA methylation levels in TEs (TE methylation), and the basal expression levels (TPM) of *TRIM28*, *SETDB1*, *PLAGL1*, *ZNF519*, *ZNF566*, and *ZNF611*. To determine top candidate KRAB-ZNF host factors, we gathered evidence of the correlation between KRAB-ZNF expression and TE accessibility post-infection, the correlation between basal KRAB-ZNF expression and viral load, and the KRAB-ZNF binding sites and motifs found in high variable families (Table S7). Here, we kept KRAB-ZNF motifs that are found in $\geq$50 accessible instances and $\geq$50% of all instances in TE peak regions per family. The family with the highest percentage was kept as the top-associated TE.

R *glm* function with the parameter *family = Gaussian()* was first used to include all variables in the generalized linear model. R *stepAIC* function was then used to choose a subset of main features for the final model. R *summary* function was used to report

the R^2, adjusted R^2 and p value. Lastly, we used the R *predict* function with the parameter *type* = *"response"* for the expected viral load with each predictive model.

QUANTIFICATION AND STATISTICAL ANALYSIS

Statistical details can be found in the corresponding section of "method details". All statistical analyses were performed in R.

ADDITIONAL RESOURCES

The study did not generate any additional resources.

Cell Genomics, Volume *3*

Supplemental information

Transposable elements are associated with the variable response to influenza infection

Xun Chen, Alain Pacis, Katherine A. Aracena, Saideep Gona, Tony Kwan, Cristian Groza, Yen Lung Lin, Renata Sindeaux, Vania Yotova, Albena Pramatarova, Marie-Michelle Simon, Tomi Pastinen, Luis B. Barreiro, and Guillaume Bourque

SUPPLEMENTARY FIGURES

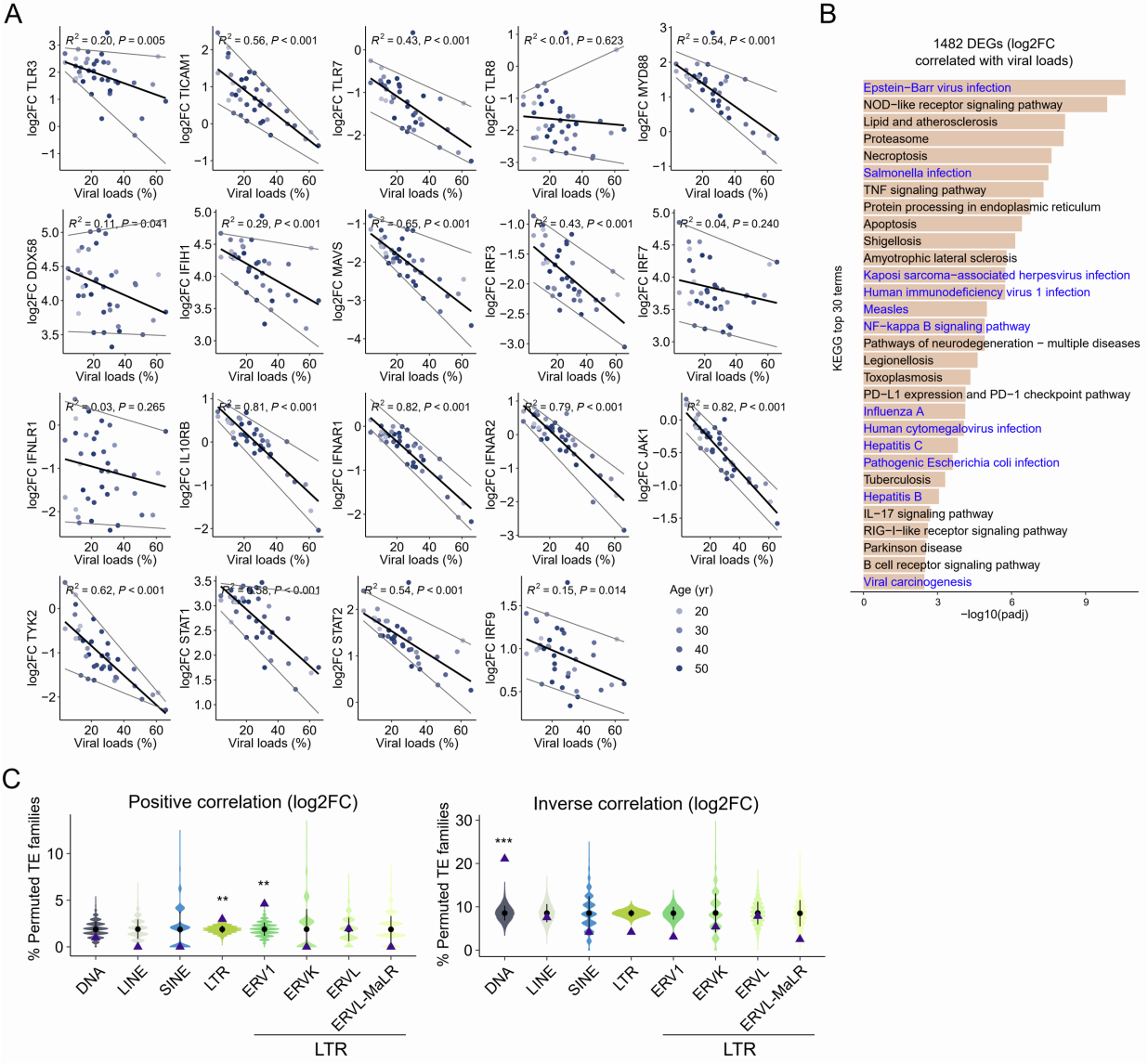

Figure S1. Immune genes and few TE families are prone to correlate with viral load post-infection, related to Figure 1

(A) Expression fold changes (log2FCs) of most key immune regulators are inversely correlated with viral load post-infection. Many genes are shown to strongly correlate with viral load, including membrane-bound receptor genes sensing infection-induced interferons, *i.e.*, *IL10RB*, *IFNAR1*, *IFNAR2*, and *JAK1*. Linear regression model was used for the correlation analysis.

Black line represents the regression line and grey lines represent the 5% and 95% quantiles. **(B)** Expression fold change amongst differentially expressed genes (DEGs) correlated with viral load are enriched in multiple virus infection pathways. 1,482 DEGs with log2FCs correlated with viral load ($R^2 \geq 0.3$, p value ≤ 0.05) were identified and used for downstream pathway enrichment analysis. **(C)** Enrichment of the proportion for log2FC amongst TE families positively and inversely correlated with viral load post-infection. 17 positively and 77 inversely correlated TE families were analyzed. Purple triangle represents the actual proportion of correlated families among subclass or superfamily. Error bar represents the mean values and standard deviations of 10,000 randomized proportions. One-tailed student's *t*-test was used to compare the actual proportions with randomized proportions (* $p \leq 0.05$, ** $p \leq 0.01$, *** $p \leq 0.001$).

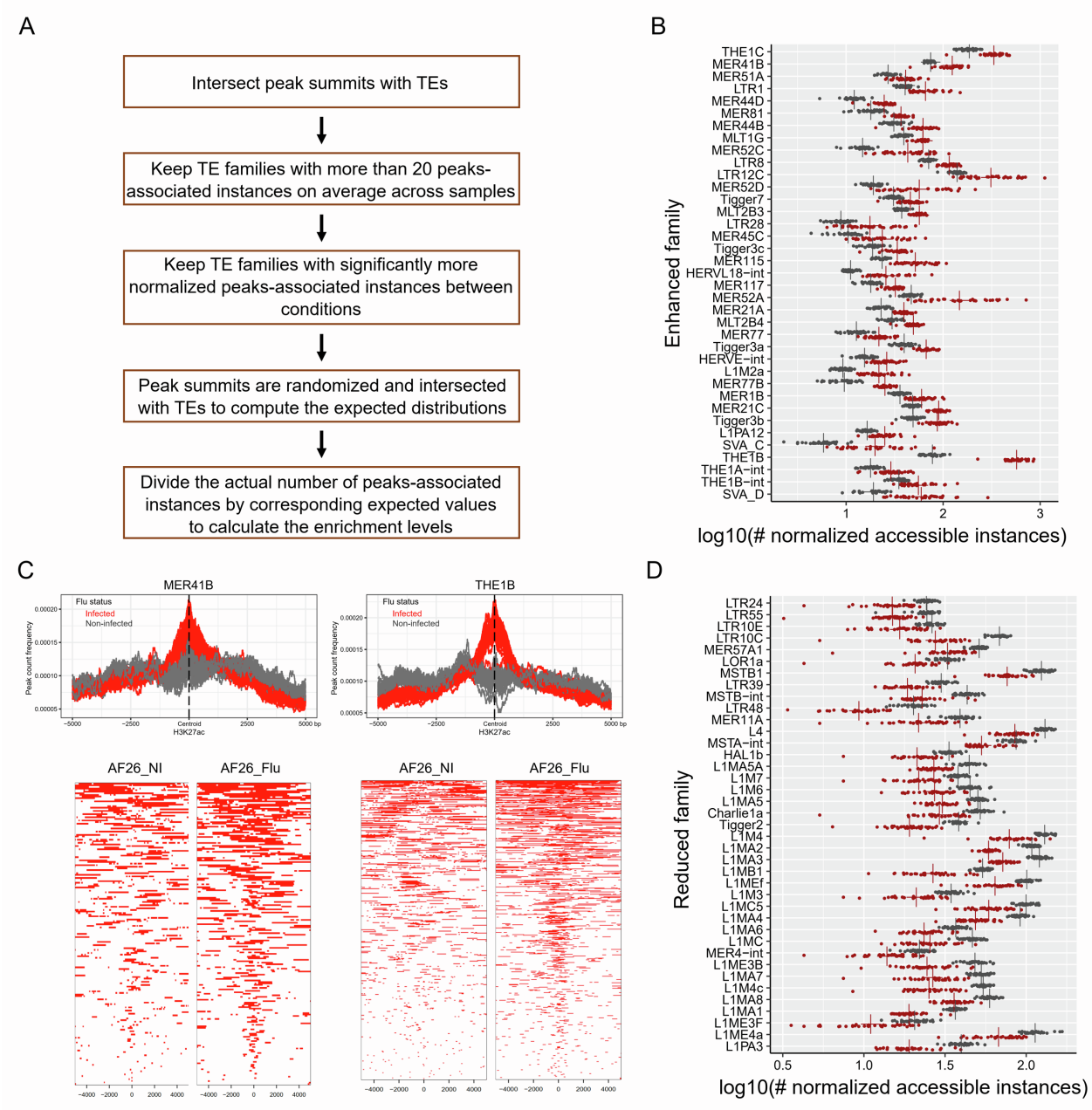

Figure S2. Detection of TE families with enhanced and reduced accessibility in response to IAV infection, related to Figure 2

(A) Optimized TE enrichment analysis pipeline. Details were described in Methods. **(B)** Distributions of the normalized number of peaks-associated instances of TE families with enhanced accessibility. Each point represents one sample. Grey color represents the non-infected

sample and red color represents the infected sample. "+" indicates the mean value across non-infected (grey) and infected (red) samples. The number of accessible instances were normalized by the average number of peaks across infected and non-infected samples, respectively. **(C)** Average profiles (up) and heatmaps (bottom) of H3K27ac peaks at MER41B and THE1B (± 5 kb). H3K27ac peaks are centered at the median positions of peak summits across infected samples. Peak regions are shown as heatmaps at the bottom. AF26 non-infected and infected samples are shown as examples. Peak regions centered at each family are shown as red bars. **(D)** Distributions of the normalized number of peaks-associated instances of TE families with reduced accessibility. Each point represents one non-infected (grey) and infected (red) sample. "+" indicates the mean value across non-infected (grey) and infected (red) samples. The number of accessible instances were normalized by the average number of peaks across infected and non-infected samples separately.

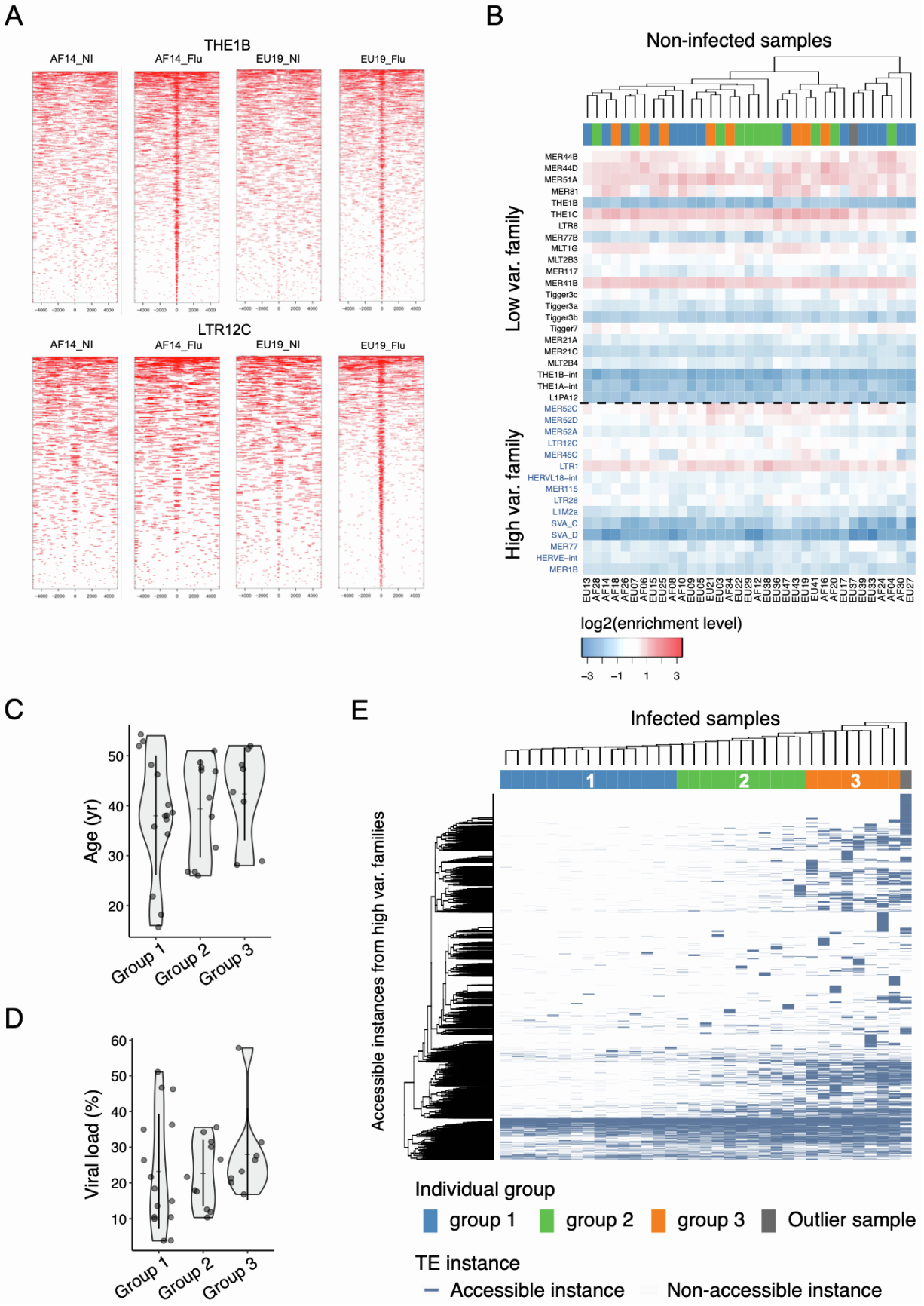
A
THE1B
AF14_NI
AF14_Flu
EU19_NI
EU19_Flu
LTR12C
AF14_NI
AF14_Flu
EU19_NI
EU19_Flu
B
Non-infected samples
Low var. family
High var. family
MER44B
MER44D
MER51A
MER81
THE1B
THE1C
LTR8
MER77B
MLT1G
MLT2B3
MER117
MER41B
Tigger3c
Tigger3a
Tigger3b
Tigger7
MER21A
MER21C
MLT2B4
THE1B–int
THE1A–int
L1PA12
MER52C
MER52D
MER52A
LTR12C
MER45C
LTR1
HERVL18–int
MER115
LTR28
L1M2a
SVA_C
SVA_D
MER77
HERVE–int
MER1B
log2(enrichment level)
–3
–1
1
3
C
Age (yr)
50
40
30
20
Group 1
Group 2
Group 3
D
Viral load (%)
60
50
40
30
20
10
Group 1
Group 2
Group 3
E
Infected samples
1
2
3
Accessible instances from high var. families
Individual group
group 1
group 2
group 3
Outlier sample
TE instance
Accessible instance
Non-accessible instance

Figure S3. High variable families display high variability in chromatin accessibility post-infection, related to Figure 3

(A) Heatmaps of open chromatin regions at THE1B and LTR12C (± 5 kb). Two infected and non-infected samples are shown as examples. LTR12C shows a high variability of accessibility between randomly-selected samples post-infection. ATAC-seq peaks are centered at the summits in TEs. 5 kb upstream and downstream regions are shown. Compared to AF14, EU19 displays a higher enrichment at LTR12C but comparable enrichment at THE1B. **(B)** Heatmap of log2 enrichment levels of 37 enhanced families in 35 non-infected samples. Semi-clustering analysis was performed. Three individual groups observed at infected samples are not clustered together. High variable families are highlighted in blue color. **(C,D)** Violin plots of age of macrophage donors and viral load of the three individual groups. Group 3 individuals have relatively older ages and higher viral load compared to group 1 individuals. The dot represents each individual and the error bar represents the mean value and standard deviation. **(E)** Heatmap of the chromatin state of accessible instances from high variable families in 35 infected samples. The state of open chromatin is in blue color and closed chromatin in white color. Unsupervised clustering analysis was performed, and the three individual groups are clustered together. A fraction of instances shows an enrichment in group 3 compared to group 1 individuals.

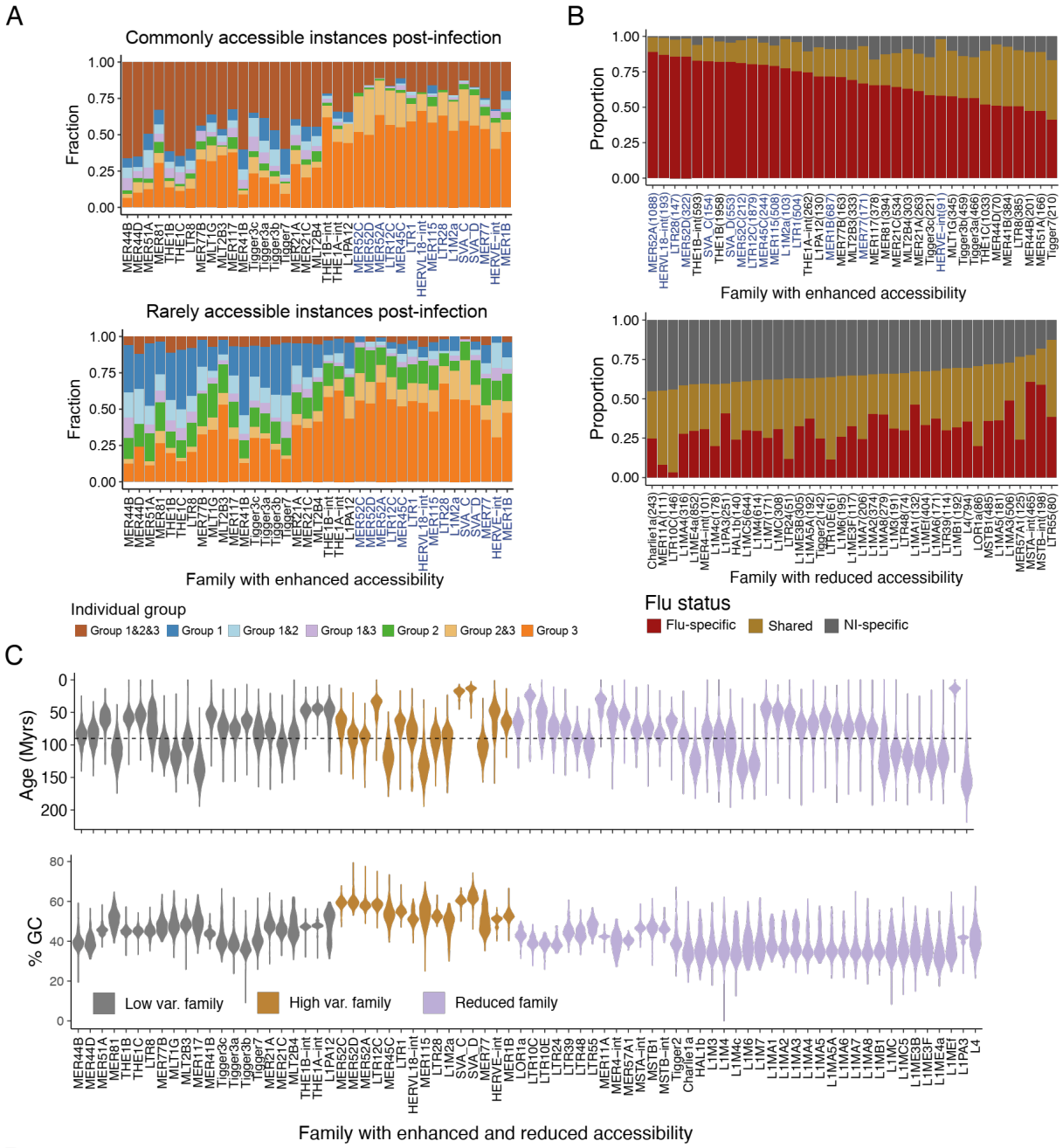
A
Commonly accessible instances post-infection
Fraction
Rarely accessible instances post-infection
Fraction
Family with enhanced accessibility
B
Proportion
Family with enhanced accessibility
Proportion
Family with reduced accessibility
Individual group
Group 1&2&3
Group 1
Group 1&2
Group 1&3
Group 2
Group 2&3
Group 3
Flu status
Flu-specific
Shared
NI-specific
C
Age (Myrs)
% GC
Low var. family
High var. family
Reduced family
Family with enhanced and reduced accessibility
D
log10(# instances in the human genome)
0.0003
Low var. families
High var. families
accessible instances
0.81
Low var. families
High var. families

Figure S4. Characteristics of TE families display high variability in chromatin accessibility post-infection, related to Figure 3

(A) Proportions of accessible instances per enhanced family are variable between three individual groups post infection. Commonly accessible instances represent instances that are accessible in more than 25% samples from at least one group (left); rarely accessible instances represent instances that are accessible in less than 25% samples from any groups (right). Enrichment in one individual group refers to instances that are accessible in more than 25% samples for commonly accessible instances and one or more samples for rarely accessible instances. High variable families are highlighted in blue color. **(B)** Proportions of flu-specific, shared, and NI-specific instances of each family with enhanced and reduced accessibility. Flu-specific instances represent instances that are accessible in ≥ 1 infected and no non-infected sample; NI-specific instances represent instances that are accessible in ≥ 1 non-infected and no infected sample; Shared instances represent instances that are accessible in ≥ 1 non-infected and ≥ 1 infected samples. High variable families are in blue color. **(C)** Violin plot of the estimated TE evolutionary ages (up) and GC contents (bottom). Dotted lines indicate the evolution time when primates diverged from other mammals (~90 million years ago). No distinct patterns are observed between high variable, low variable families, and reduced families. The estimation of ages was described in Methods. High variable families show a higher GC content compared to others. Group 3 individuals have comparable or lower GC content than other individuals, supporting that the higher accessibility in high variable families for group 3 individuals are not derived from sequencing artifacts. **(D)** Number of instances and accessible instances from high variable and low variable families. *P* values computed by two-tailed student's *t*-test are shown above the dot plots.

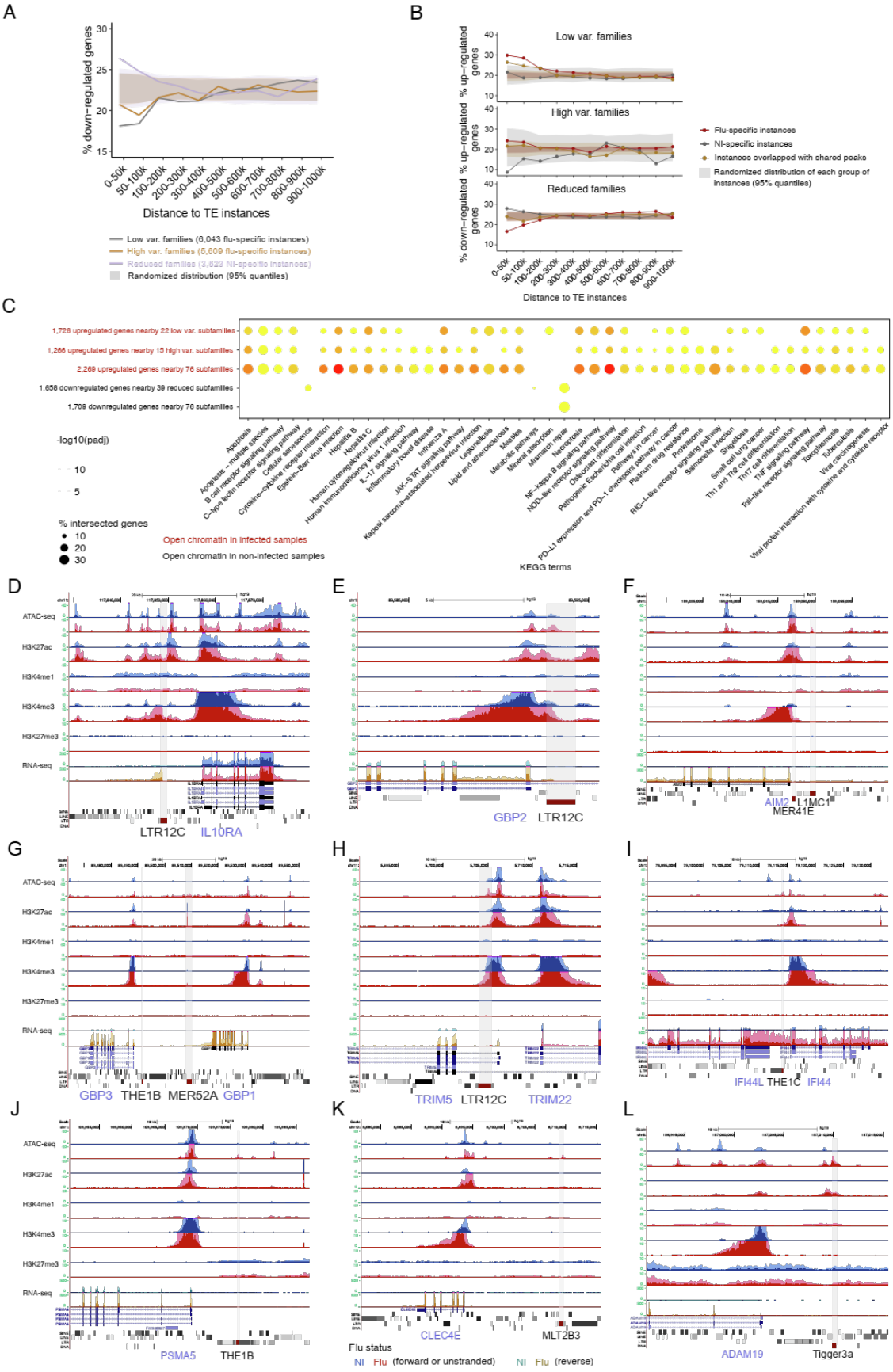
A
% down−regulated genes
Distance to TE instances
0-50k
50-100k
100-200k
200-300k
300-400k
400-500k
500-600k
600-700k
700-800k
800-900k
900-1000k
Low var. families (6,043 flu-specific instances)
High var. families (5,609 flu-specific instances)
Reduced families (3,823 NI-specific instances)
Randomized distribution (95% quantiles)
B
Low var. families
High var. families
Reduced families
% up−regulated genes
% down−regulated genes
Distance to TE instances
Flu-specific instances
NI-specific instances
Instances overlapped with shared peaks
Randomized distribution of each group of instances (95% quantiles)
C
1,726 upregulated genes nearby 22 low var. subfamilies
1,286 upregulated genes nearby 15 high var. subfamilies
2,269 upregulated genes nearby 76 subfamilies
1,658 downregulated genes nearby 39 reduced subfamilies
1,709 downregulated genes nearby 76 subfamilies
-log10(padj)
10
5
% intersected genes
10
20
30
Open chromatin in infected samples
Open chromatin in non-infected samples
Apoptosis
Apoptosis − multiple species
B cell receptor signaling pathway
C−type lectin receptor signaling pathway
Cellular senescence
Cytokine−cytokine receptor interaction
Epstein−Barr virus infection
Hepatitis B
Hepatitis C
Human cytomegalovirus infection
Human immunodeficiency virus 1 infection
IL−17 signaling pathway
Inflammatory bowel disease
Influenza A
JAK−STAT signaling pathway
Kaposi sarcoma−associated herpesvirus infection
Legionellosis
Lipid and atherosclerosis
Measles
Metabolic pathways
Mineral absorption
Mismatch repair
Necroptosis
NF−kappa B signaling pathway
NOD−like receptor signaling pathway
Osteoclast differentiation
Pathogenic Escherichia coli infection
Pathways in cancer
PD−L1 expression and PD−1 checkpoint pathway in cancer
Platinum drug resistance
Proteasome
RIG−I−like receptor signaling pathway
Salmonella infection
Shigellosis
Small cell lung cancer
Th1 and Th2 cell differentiation
Th17 cell differentiation
TNF signaling pathway
Toll−like receptor signaling pathway
Tuberculosis
Viral carcinogenesis
Viral protein interaction with cytokine and cytokine receptor
KEGG terms
D
E
F
ATAC-seq
H3K27ac
H3K4me1
H3K4me3
H3K27me3
RNA-seq
LTR12C
IL10RA
GBP2
LTR12C
AIM2
L1MC1
MER41E
G
H
I
GBP3
THE1B
MER52A
GBP1
TRIM5
LTR12C
TRIM22
IFI44L
THE1C
IFI44
J
K
L
PSMA5
THE1B
CLEC4E
MLT2B3
ADAM19
Tigger3a
Flu status
NI Flu (forward or unstranded)
NI Flu (reverse)

Figure S5. TE families with accessibility changes may co-opt in the immune response to IAV infection, related to Figure 4

(A) Fractions of down-regulated genes near accessible TEs relative to the random distributions. Proportions of down-regulated genes are shown within each of the genomic intervals relative to nearby accessible TEs. More details were described in **Figure 4A**. **(B)** Proportions of up/down-regulated genes near flu-specific, NI-specific, and shared instances. Proportions were computed within each of the genomic intervals relative to nearby accessible instances. Upregulated genes were analyzed for high variable and low variable families, and downregulated genes were analyzed for reduced families. Expected distributions were computed as we described in Methods (shaded regions, 95% confidence intervals). The proportions were compared with corresponding expected distributions. Flu-specific instances from low variable and high variable families and NI-specific instances from reduced families display the highest proportions of up/down-regulated genes within 100 kb relative to nearby accessible instances, particularly within 50 kb. **(C)** Pathway enrichment analysis of DEGs adjacent (≤ 50 kb) to each category of families. It shows the enrichment of multiple immune-related pathways near families with enhanced accessibility. Some pathways are differentially enriched between high variable and low variable families, including RIG-I-like receptor signaling pathway. **(D)** Genomic view of an accessible LTR12C with the expression was upregulated and initiated at the open chromatin region post-infection. The LTR12C instance highlighted as the shaded area shows an upregulated accessibility, expression, and H3K4me3 activity. *IL10RA* gene located near the LTR12C instance is also significantly upregulated post-infection. **(E-L)** Example genomic views of instances with enhanced accessibility post-infection. Instances are highlighted as the shaded areas. Eight TE immune-related gene pairs are shown, i.e., LTR12C-*GBP2*, MER41-*AIM2*, MER52A/THE1B-

GBP1/3, LTR12C-*TRIM22*, THE1C-*IFI44*, THE1B-*PSMA5*, and MLT2B3-*CLEC4E*, and Tigger3a-*ADAM19*. *GBP2* has been validated to be regulated by the upstream LTR12C instance.[1] *AIM2* has also been validated to be regulated by a MER41 instance;[2] interestingly, it may also be regulated by another TE instance. Other three TE instances reported by Chuong et al.[2] that potentially regulate *APOL1*, *IFI6*, and *SECTM1* did not show chromatin change in macrophages (https://computationalgenomics.ca/tools/epivar). The dark shaded area denotes the distribution of the average RPM values and the light shaded area denotes the standard deviation. Signals of various epigenetic marks are shown in blue color for non-infected samples and red color for infected samples. For RNA-seq, forward and reverse transcripts are shown in blue and green color separately for non-infected samples; while forward and reverse transcripts are shown in red and brown color separately for infected samples.

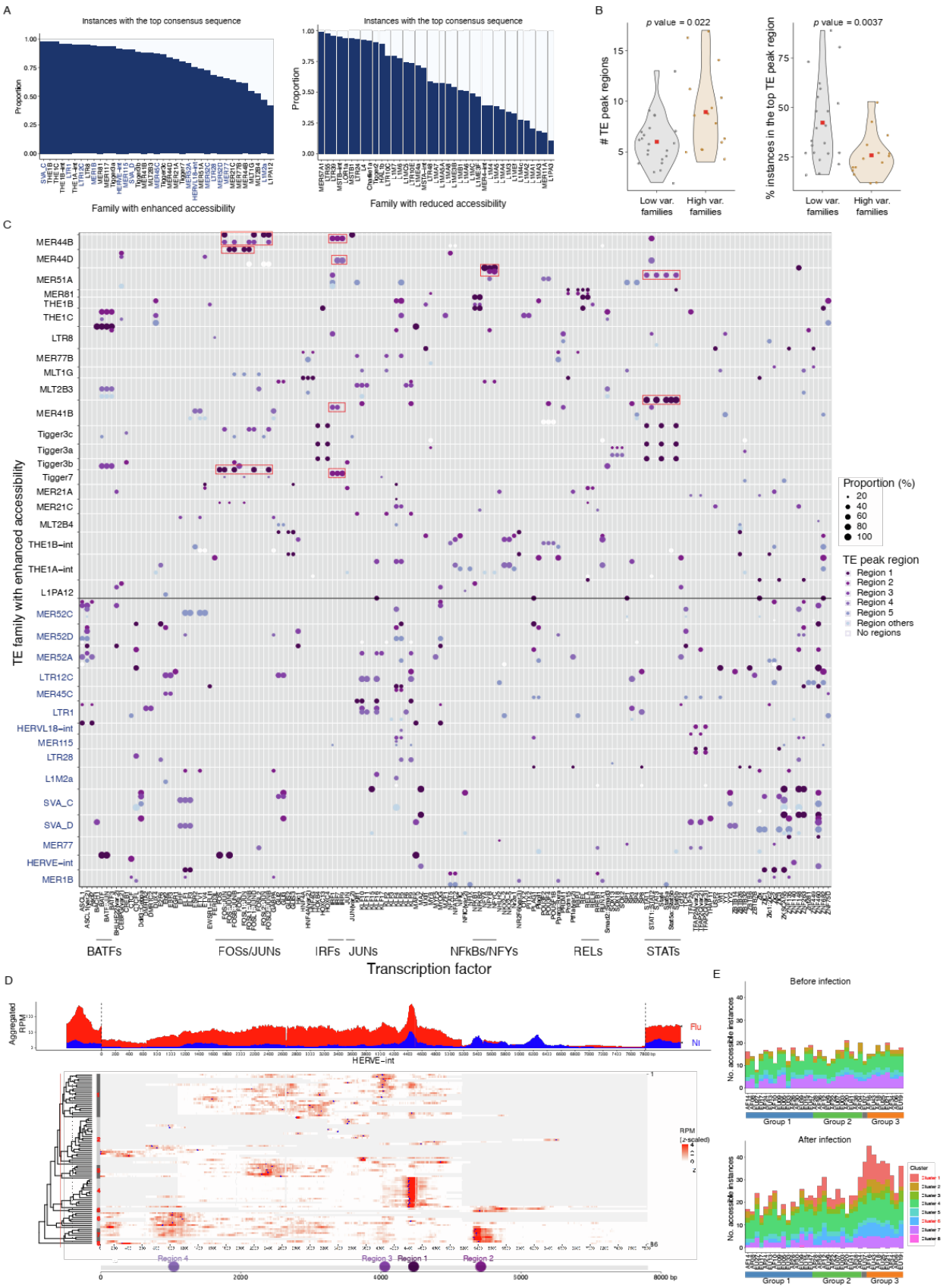
A
Instances with the top consensus sequence
Proportion
Family with enhanced accessibility
Instances with the top consensus sequence
Proportion
Family with reduced accessibility
B
p value = 0.022
TE peak regions
Low var. families
High var. families
p value = 0.0037
% instances in the top TE peak region
Low var. families
High var. families
C
TE family with enhanced accessibility
MER44B
MER44D
MER51A
MER81
THE1B
THE1C
LTR8
MER77B
MLT1G
MLT2B3
MER41B
Tigger3c
Tigger3a
Tigger3b
Tigger7
MER21A
MER21C
MLT2B4
THE1B–int
THE1A–int
L1PA12
MER52C
MER52D
MER52A
LTR12C
MER45C
LTR1
HERVL18–int
MER115
LTR28
L1M2a
SVA_C
SVA_D
MER77
HERVE–int
MER1B
BATFs
FOSs/JUNs
IRFs
JUNs
NFkBs/NFYs
RELs
STATs
Transcription factor
Proportion (%)
20
40
60
80
100
TE peak region
Region 1
Region 2
Region 3
Region 4
Region 5
Region others
No regions
D
Aggregated RPM
HERVE–int
Flu
NI
RPM [z-scaled]
Region 4
Region 3
Region 1
Region 2
E
Before infection
No. accessible instances
Group 1
Group 2
Group 3
After infection
No. accessible instances
Cluster
Group 1
Group 2
Group 3

Figure S6. TE peak regions and TF binding motifs reveal the association of high variability in chromatin accessibility with KRAB-ZNFs, related to Figure 5

(A) Proportions of accessible instances with top candidate consensus sequences. Consensus sequence information was achieved from the ".align" files generated by RepeatMasker. It shows a high proportion for TE families with enhanced accessibility. High variable families are highlighted in blue color. **(B)** Number of TE peak regions detected for high variable and low variable families. Compared to low variable families, high variable families have significantly more TE peak regions and more instances in the top TE peak region. *P* values were computed by the two-tailed student's *t*-test. **(C)** TF binding motifs enriched in each TE peak region of families with enhanced accessibility. Top five TE peak regions are shown. Instances in other regions and instances not within TE peak regions were analyzed separately. TE peak regions of each family are shown as separate rows. Dot size refers to the proportion of instances in each region containing each motif. Dotted line separates high variable and low variable families and high variable families are also highlighted in blue color. **(D)** Aggregated RPM (up) and RPM (bottom) values on each instance along the HERVE-int consensus sequence. Infected (red) and non-infected (blue) samples are shown separately including the upstream and downstream regions (± 20% of the consensus sequence length). Computed RPM values were *z*-scaled in the heatmap while values below zero are in white color. Deletions relative to the consensus sequence are shown in grey color. Unsupervised clustering analysis was performed with the scaled RPM values to determine the main clusters. Blue triangles indicate the peak centroids referring to the highest RPM values. TE peak regions and positions are shown in the bottom (Same as **Figure 5B**). More details were described in Methods. **(E)** Number of accessible instances from each cluster. Infected and non-infected samples are shown separately. Individuals are ordered based

on the clustering obtained in **Figure 3C**. Instances from Cluster 1 and 6, most of which contain TE peak region 3 and 4, are more abundant in group 3 individuals than group 1 individuals.

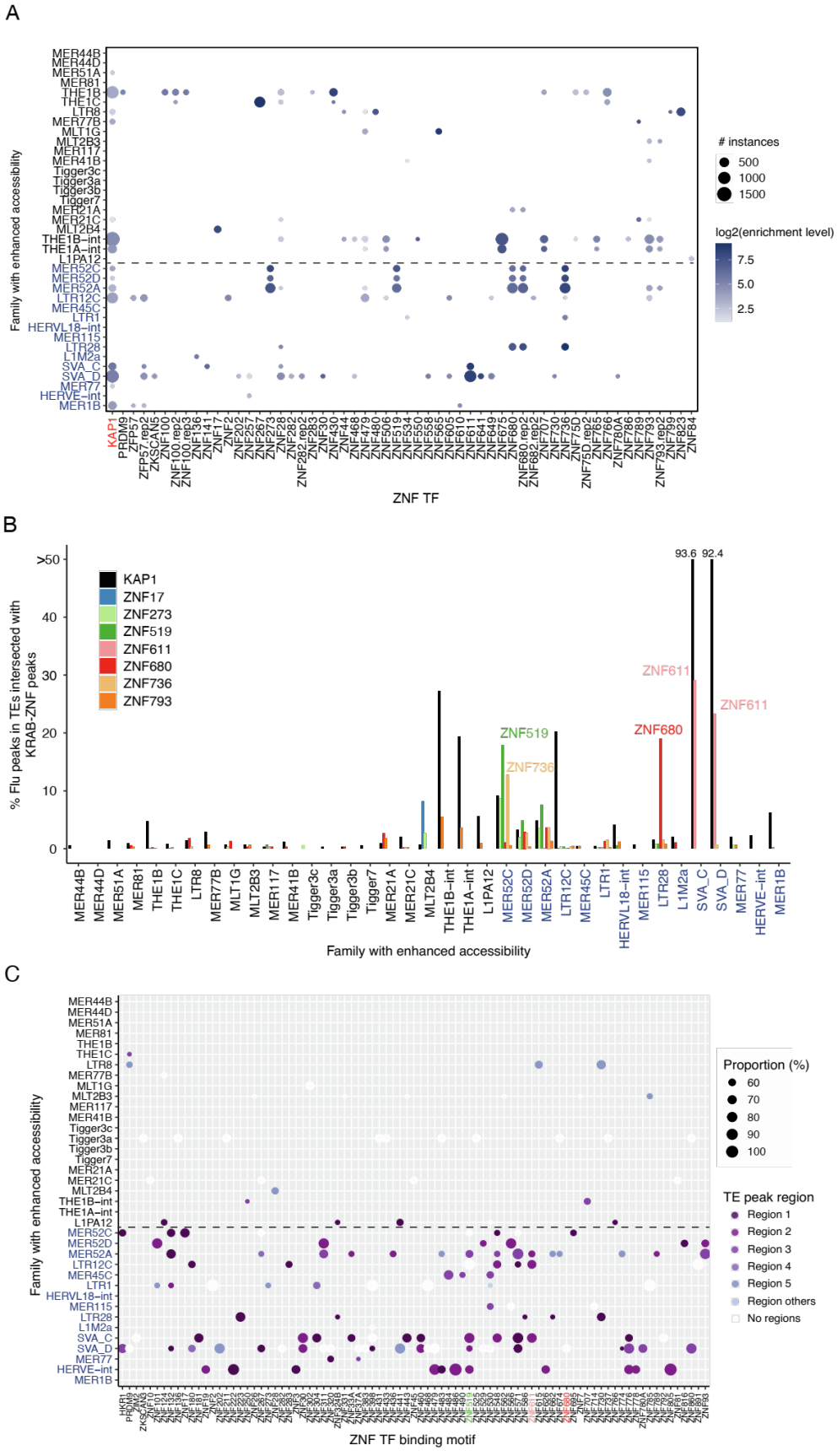
A
Family with enhanced accessibility
ZNF TF
instances
500
1000
1500
log2(enrichment level)
7.5
5.0
2.5
B
% Flu peaks in TEs intersected with KRAB-ZNF peaks
Family with enhanced accessibility
KAP1
ZNF17
ZNF273
ZNF519
ZNF611
ZNF680
ZNF736
ZNF793
93.6
92.4
ZNF611
ZNF611
ZNF680
ZNF519
ZNF736
C
Family with enhanced accessibility
ZNF TF binding motif
Proportion (%)
60
70
80
90
100
TE peak region
Region 1
Region 2
Region 3
Region 4
Region 5
Region others
No regions

Figure S7. KAP1 and KRAB-ZNFs are associated with high variability in chromatin accessibility in high variable families, related to Figure 5

(A) Enrichment levels of KRAB-ZNF binding sites in high variable and low variable families in 257 HEK293T cell lines.[3] High variable families like MER52s, SVAs, LTR12C, and LTR28 are shown to be enriched for KRAB-ZNF binding sites. Color intensity refers to the fold enrichment relative to the random distribution (see Methods). (**B**) Proportion of KAP1 and KRAB-ZNF binding sites that overlap with accessible regions in TEs post-infection. A 100-bp of genomic region centered at the ATAC-seq peak centroids was used for this analysis. KRAB-ZNFs with a minimum of 5% across enhanced families were visualized. **(C)** KRAB-ZNF binding motifs enriched in enhanced families. Motifs were obtained from Barazandeh et al.[4] Same motifs enriched across TE peak regions are aggregated. TE peak regions with the most instances are shown as representatives. KRAB-ZNFs with their enrichment of binding sites in high variable families are highlighted.

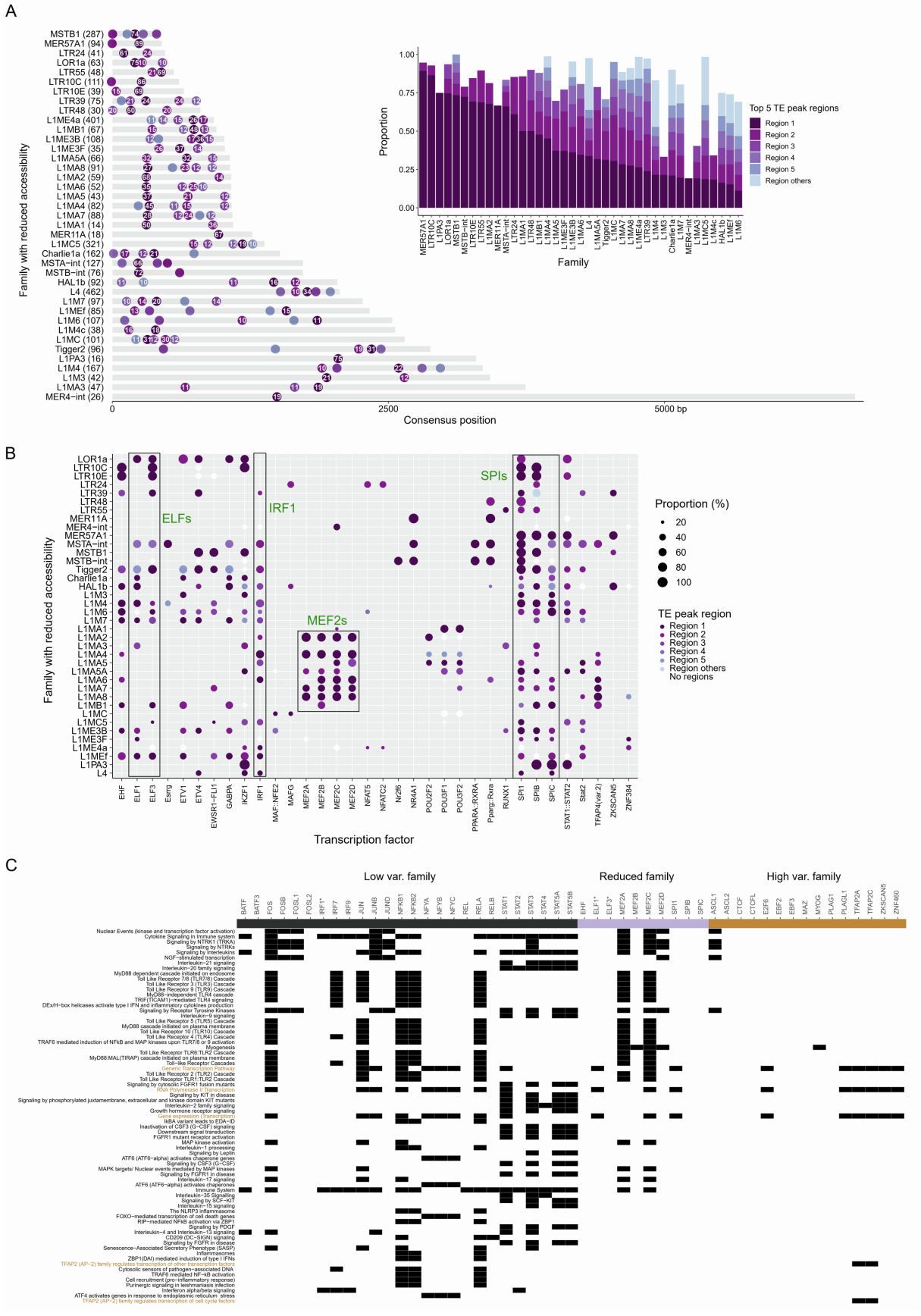
A
Family with reduced accessibility
Consensus position
0
2500
5000 bp
Proportion
Family
Top 5 TE peak regions
Region 1
Region 2
Region 3
Region 4
Region 5
Region others
B
Family with reduced accessibility
Transcription factor
ELFs
IRF1
MEF2s
SPIs
Proportion (%)
TE peak region
Region 1
Region 2
Region 3
Region 4
Region 5
Region others
No regions
C
Low var. family
Reduced family
High var. family

Figure S8. TE Peak regions and TF binding motifs enriched in reduced families and different sets of TE families may co-opt in distinct regulatory pathways in response to IAV infection, related to Figure 5

(A) Distribution and TE peak regions on reduced families. The inset barplot shows the proportion of instances in each TE peak region. The locations and proportions (%) of the top-five TE peaks regions along the consensus sequence are shown. The number in each dot refers to the proportion (above 10%) among accessible instances in each TE peak region. It shows that most instances with reduced accessibility (in Region 1) from L1MA families are consistently located at similar locations of the 3'end of consensus sequence. Y-axis shows the family name and the number of accessible instances mapped to the top consensus sequence. TE peak regions were detected as we described in Methods. **(B)** TF binding motifs enriched in reduced families. Same motifs enriched across TE peak regions were aggregated and the proportions of instances containing each motif are shown. TE peak regions with more accessible instances are shown as representatives. Black boxes highlighted the SPI and MEF2 related motifs (green color) enriched in reduced families. It shows that Region 1s (located at around 300 bp, **Figure S6B**) of L1MA families are consistently enriched for MEF2 related motifs. MEF2 related TFs were previously reported to regulate anti-microbial genes.[5] **(C)** TFs potentially bound to different categories of families are involved in distinct pathways. Apart from AP-2 related pathways, TFs bound to high variable families are mainly involved in transcription-related pathways. TFs bound to low variable families and reduced families are mainly involved in cytokine signaling and other immune-related pathways. Bars in different colors represent different categories of families they are enriched. * indicates motifs that are enriched in different categories of families. IRF1 motif is

enriched in both low variable families and reduced families. ELF1/3 motifs are enriched in both high variable families and reduced families.

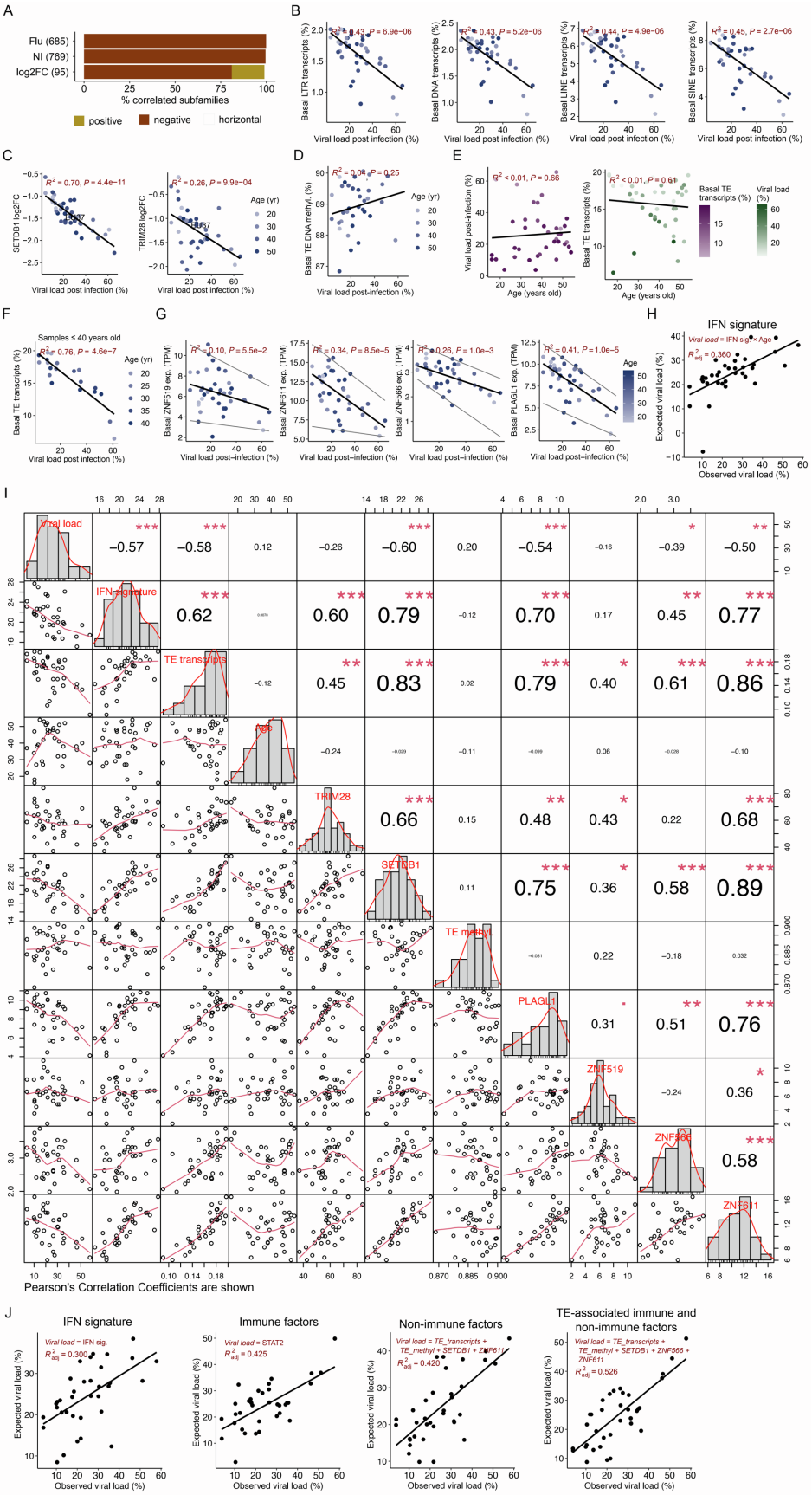
A
Flu (685)
NI (769)
log2FC (95)
% correlated subfamilies
positive
negative
horizontal
B
Basal LTR transcripts (%)
Basal DNA transcripts (%)
Basal LINE transcripts (%)
Basal SINE transcripts (%)
Viral load post infection (%)
C
SETDB1 log2FC
TRIM28 log2FC
Age (yr)
D
Basal TE DNA methyl. (%)
E
Viral load post-infection (%)
Basal TE transcripts (%)
Age (years old)
F
Samples ≤ 40 years old
G
Basal ZNF519 exp. (TPM)
Basal ZNF611 exp. (TPM)
Basal ZNF566 exp. (TPM)
Basal PLAGL1 exp. (TPM)
H
IFN signature
Expected viral load (%)
Observed viral load (%)
I
Viral load
IFN signature
TE transcripts
Age
TRIM28
SETDB1
TE methyl.
PLAGL1
ZNF519
ZNF566
ZNF611
Pearson's Correlation Coefficients are shown
J
IFN signature
Immune factors
Non-immune factors
TE-associated immune and non-immune factors

Figure S9. Correlations between TE-associated host factors and viral load post-infection, related to Figure 6

(A) Correlation directions among TE families that are correlated ($R^2 \geq 0.3$ and p value ≤ 0.05) with viral load post-infection (**Figure 6A**). More details were described in Methods. **(B)** Consistent inverse correlations between the basal transcripts of four main TE subclasses and viral load, including LTR, DNA, LINE, and SINE. The basal amount of transcript refers to the proportion of aggregated normalized read counts in each subclass among the global transcripts. Black line represents the regression line. R^2 and p values computed by the linear regression model are shown. **(C)** Correlations between the expression fold changes (log2FCs) of both *SETDB1* (left) and *TRIM28* (right) and viral load. *SETDB1* rather than *TRIM28* is shown to be inversely correlated with viral load. **(D)** Correlation between the basal DNA methylation level in TEs and viral load. Individuals with low viral load are likely to have lower TE DNA methylation levels. **(E)** Correlations between both viral load post-infection (left) and basal TE transcripts (right) and ages. Samples from younger individuals have a relatively higher amount of basal TE transcripts with a smaller deviation compared to older samples in macrophages. Two samples were identified as outliers having among the lowest amount of basal TE transcripts; strikingly, they also preserved among the highest viral load. **(F)** Correlation between the basal TE transcripts and viral load for individuals 40 years old or younger. It shows an increased correlation compared to the correlation among 39 samples (**Figure 6B**). **(G)** Correlations between the basal expression of candidate host factors and viral load post-infection. Basal *ZNF519*, *ZNF566*, *ZNF611* and *PLAGL1* expressions are both inversely correlated with viral load post-infection. **(H)** Multivariable regression model developed for the predictive of viral load post-infection using type I interferon (IFN) signature and age only. Details were described in

Methods. **(I)** Correlation matrix chart of viral load and variables that are potentially associated with IAV infection and TEs. Histograms and kernel density overlays of each variable are shown. Scatterplot matrix and absolute correlations between each of two variables and viral load are also shown. Red lines represent the distribution. R *chart.Correlation* function was used for the analysis. Pearson's correlation coefficients are shown (* $p \leq 0.05$, ** $p \leq 0.01$, *** $p \leq 0.001$). **(J)** Multivariable regression models developed for the predictive of viral load post-infection while age was included as an independent variable. We used the same sets of variables for the models included in **Figure S9H** and **Figure 6H-J**. The adjusted R^2 is significantly lower than the model developed by the inclusion of age as an interaction term variable. Details were described in Methods.

REFERENCES

1. Srinivasachar Badarinarayan, S., Shcherbakova, I., Langer, S., Koepke, L., Preising, A., Hotter, D., Kirchhoff, F., Sparrer, K.M.J., Schotta, G., and Sauter, D. (2020). HIV-1 infection activates endogenous retroviral promoters regulating antiviral gene expression. Nucleic Acids Research *48*, 10890–10908. 10.1093/nar/gkaa832.

2. Chuong, E.B., Elde, N.C., and Feschotte, C. (2016). Regulatory evolution of innate immunity through co-option of endogenous retroviruses. Science *351*, 1083–1087. 10.1126/science.aad5497.

3. Imbeault, M., Helleboid, P.-Y., and Trono, D. (2017). KRAB zinc-finger proteins contribute to the evolution of gene regulatory networks. Nature *543*, 550–554. 10.1038/nature21683.

4. Barazandeh, M., Lambert, S.A., Albu, M., and Hughes, T.R. (2018). Comparison of ChIP-Seq Data and a Reference Motif Set for Human KRAB C2H2 Zinc Finger Proteins. G3 Genes|Genomes|Genetics *8*, 219–229. 10.1534/g3.117.300296.

5. Clark, R.I., Tan, S.W.S., Péan, C.B., Roostalu, U., Vivancos, V., Bronda, K., Pilátová, M., Fu, J., Walker, D.W., Berdeaux, R., et al. (2013). MEF2 Is an In Vivo Immune-Metabolic Switch. Cell *155*, 435–447. 10.1016/j.cell.2013.09.007.